國 立 交 通 大 學
顯 示 科 技 研 究 所

碩士學位論文

藉由長共振腔極大反常色散摻鉺光纖鎖模雷射來產生高能量脈衝

High energy pulse generation in large negative-dispersion mode-locked Er-doped fiber laser with long cavity length

研究生:甘力行

指導教授: 賴暎杰 教授

中華民國一百年六月

摘要

論文名稱：藉由長共振腔極大反常色散摻鉺光纖鎖模雷射來產生高能量脈衝

校所別：國立交通大學顯示科技研究所　　頁數：1 頁

畢業時間：九十九學年度第二學期　　學位：碩士

研究生：甘力行　　指導教授：賴暎杰教授

在本論文中，我們研究一套操作在超大異常色散之摻鉺光纖被動鎖模雷射系統的輸出特性。雷射共振腔長約 400 公尺，可產生 500kHz 超低脈衝重複頻率，利用不同的輸出耦合率，可直接輸出超過 120nJ 高能量穩定脈衝序列。藉由適當調整輸入之功率與偏振控制器之角度可得到穩定不分裂之方波輸出,最後透過脈衝寬度與頻寬計算可得出此雷射輸出之特性參數來估計脈寬壓縮的資訊。

ABSTRACT

Title：High energy pulse generation in large negative-dispersion mode-locked Er-doped fiber laser with long cavity length

Pages：1 Page

School：National Chiao Tung University

Department：Display Institute

Time：June, 2011 Degree：Master

Researcher：Li-Hsing Kan Advisor：Prof. Yinchieh Lai

In this thesis, we experimentally demonstrate a passive mode-locked Erbium-doped fiber laser with large net round trip anomalous dispersion and nonlinearity through about 400m cavity length. The laser can output optical pulse trains at the low repetition rate around 500kHz and with the high pulse energy larger than 120nJ directly from the laser output. By adjusting the polarization controllers (PCs) and the pump power level, high energy pulses with square profile and nanosecond pulse-width without pulse breaking can be observed. Finally, we study the characteristic parameters of our pulses for further compressing the pulse-width to attain the short pulse-width and high peak power.

誌謝

此篇論文能夠順利完成首先必須要感謝我的指導老師 賴暎杰老師，在我碩士班兩年期間給予的指導與照顧，讓從電子背景出生且從未接觸過光學的我能夠快速進入狀況，從賴老師身上學到的不僅是專業知識，還有許多做研究應有的態度與面對問題的解決能力，這都是我碩士班期間對大的收穫。

特別感謝林家弘老師和鞠曉山學長在實驗上的帶領與指教，讓我的實驗能夠順利完成。謝謝實驗室項維巍學長、徐桂珠學姊、郭立強學長、許宜蓁學姊、吳尚穎學長、張家豪學長、呂柏萱學長、黃柏崴學長還有何姿媛學姊在實驗以及課業上給予的幫助與建議，使我受益良多。還有感謝實驗室的夥伴 聖閔、良愉、國豪陪伴我一同努力、玩樂與分享生活中大小事情，讓我度過難忘的碩班兩年。

最後，要感謝我最親愛的父母與家人，謝謝你們不變的支持與關心，永遠在背後給予我最大的動力，讓我可以放心地衝刺我的學業，在此獻上我無限的感謝。

CONTENTS

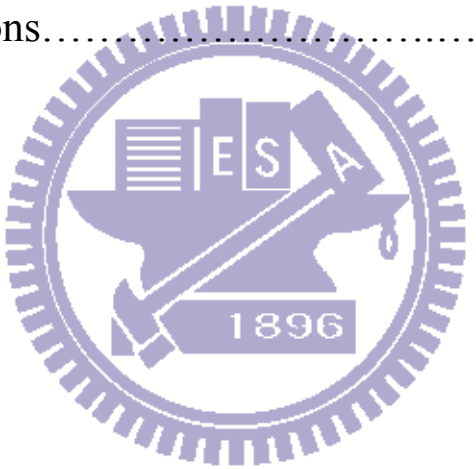

List of Figures

Chapter 1

Introduction

1.1 Passive mode-lock fiber laser

Optical fiber lasers were first demonstrated in the 1960s. Since then they have been developed to become versatile optical sources with many desirable properties. Fiber lasers have the advantages of better qualities, greater efficiency and lower sensitivity to alignment. In contrast with bulk lasers, the pump intensity in the fiber waveguide is largely independent of the laser length, resulting in large amplifier gain and low laser threshold. In the development of the Erbium Doped Fiber Amplifiers (EDFAs) in 1980s, the fiber laser researches also have drawn serious attention in the world. Since then fiber lasers have been predominantly developed for communication applications, in which many of the applications have relied on utilizing a mode-locking mechanism to produce short optical pulses.

The field of mode-locked fiber lasers has grown tremendously over the last 20 years [1.1].This class of lasers offers a low cost, rugged and compact source of ultra-short pulses. The term “mode-locking” refers to the requirement of phase-locking many different longitudinal modes of a laser cavity. If the individual phase of the light waves in each mode is not fixed, it may interference the other modes and leads to random fluctuations in the output intensity. These effects will cause the laser to be in a continuous wave (cw) operation. In case sufficiently many longitudinal modes are locked together with only small phase differences between the individual modes, it results in a continuous train of extremely short pulses rather than a CW of light.

There are two common techniques for achieving mode-locked lasers: active

and passive mode-locking. The distinction between the two techniques is that the passive methods rely on the exploitation of nonlinear optical effects in materials to initiate mode-locking without an external signal, while the active methods typically involve using an externally modulated media or device (ex: optical modulators). General speaking, passive mode-locked lasers could generate much shorter pulses than active mode-locked lasers. It is because the active methods are limited to the speed of electronic signal generators while the passive ones can fastly modulate the absorption through the pulse-induced nonlinear effects. Several different physical mechanisms can be used for passive mode-locking: semiconductor saturable absorber mirrors (SESAM), polarization additive pulse mode-locking (P-APM) configurations and nonlinear optical loop mirrors (NOLM).

Semiconductor saturable absorber mirror (SESAM) technology has been widely used to attain the mode-locking regime in different solid-state and fiber lasers. Femtosecond mode-locked lasers utilizing SESAM have been demonstrated [1.2]. The SESAM is a saturable absorber that operates mostly in reflection modes, and the reflectivity increases with higher incoming pulse intensity.

The polarization additive pulse mode-locking (P-APM) techniques were developed in about 1990s. Since it has many advantages and can achieve good performance, P-APM gradually replaced the real saturable absorbers, such as SESAMs. The pulse-shortening strength could be adjusted by simply rotating the polarization controllers. To date, P-APM is the most commonly used techniques to generate pulses with durations below 100fs both in the Er-fiber and Yb-fiber lasers [1.3].

The nonlinear optical loop mirror (NOLM) technique is a useful method for

many applications in optical signal processing such as pulse shaping and optical switching. It can also be used in the fiber laser to generate the mode-locking state, producing optical pulses around 100fs with high energy [1.4]. This optical device splits the input light into the two directions in the opposite ways around a fiber loop with a coupler. The two lights acquire different phases because of the nonlinear propagation in the waveguide loop and interfere again in the coupler to obtain the additive pulse mode-locking effects.

1.2 High energy pulse generation

For many applications of mode-locked fiber lasers, the peak power of the optical pulse train is one of main issues. To achieve a high power laser, many research groups have involved in this exciting research field. High pulse energy laser has many scientific and industrial applications, including biological metrology, industrial processing, remote sensing, and coherent lidar systems, etc. The pulse energy directly measured from typical mode-locked fiber lasers without external amplification is usually limited by the various characteristics of mode-locked fiber lasers. When the pumping power is increased above certain threshold, pulse breaking might occur and severely limit the achievable output pulse energy.

In order to improve the pulse energy performance, several approaches have been reported in the previous literatures. The combination of Q-switching and mode-locking in one cavity is successfully employed for generating high-energy pulses of laser radiation [1.5]. Using additional optical amplifiers is a feasible method, such like the chirped-pulse amplification (CPA) technique [1.6]. Another way to increase pulse energy of output radiation is the usage of a long

laser cavity [1.7][1.8]. The pulse repetition rate of a mode-locked laser is inversely proportional to its resonator length. The longer cavity length leads to the lower repetition rate and the higher pulse energy. The other methods including different coupling ratio, the usage of large area mode fibers [1.9][1.10] and Kerr-lens mode-locked lasers [1.11].

1.3 Square pulses generation

In the fiber laser systems, the nonlinear polarization evolution (NPE) mode-locking mechanism is one of the important techniques that we usually used. Square-like pulses can be obtained under the normal dispersion region using the NPE technique with elongation of cavity length in an all-fiber passive mode-locked Er-doped fiber laser [1.12]. According to the theory, the generation of square pulses might be due to peak clamping effect in the long cavity length laser. The high energy square pulse output can be potentially used for fiber optical sensor and laser lidar systems. In the all normal dispersion region, the square-profile dissipative solitons with the pulse energy about 281.2 nJ without pulse breaking have been experimentally reported [1.13]. Recently, in some researches the dispersion compensation fibers (DCF) have replaced the traditional single mode fibers (SMF) for increasing the cavity length in Er-doped fiber lasers. It is because the SMF exhibits anomalous dispersion within the spectrum range of Er-doped fiber lasers and the DCF could operate the laser in the net normal dispersion region. In the anomalous dispersion region, the nanosecond square pulses obtained with the long-cavity fiber ring laser and high pulse energy have also been reported [1.14]. Furthermore, operating the laser in the ultra-large negative dispersion regime might produce the dual-wavelength

step-like pulses [1.15]. To date the value of highest pulse energy for long cavity length passive mode-locked Er-doped fiber lasers at large anomalous dispersion region is reported to be around 80 nJ using traditional conventional single mode fibers.

1.4 Motivation of the thesis

Passive mode-locked lasers (PML) that can output ultra-short pulse trains are widespread to various scientific and engineering fields because their fiber delivery and high reliability. In order to develop more applications, the generation of high energy pulses directly from the laser output is increasingly required. Nevertheless, for avoiding pulse breaking or multiple pulse operation, the highest pulse energy operated in the slightly net anomalous dispersion region is quite limited [1.16]. Recently, PML lasers with both the Erbium and Ytterbium doped gain fibers have operated in the all normal dispersion configurations or in the net normal dispersion region to generate high pulse energy. High power PML Er-doped fiber lasers in the all-normal dispersion have been experimentally demonstrated [1.17]. As reported, 191 kHz and 690 kHz low repetition rate pulses with higher energy pulses over 20 nJ and 75.2 nJ can be produced in an all fiber PML ytterbium doped fiber laser in ring and linear cavity configurations respectively [1.18][1.19]. In contrast, utilization of mode-locked fiber laser operated in the large anomalous dispersion region is less investigated.

In this work, we have used the Erbium-doped fibers as the gain media to build an all-fiber laser mode-locked by the nonlinear polarization rotation mechanism. A long section of 400 m single mode fiber in the cavity is used to

build the large net round-trip amorous dispersion and net round-trip optical Kerr nonlinearity. The high energy pulses as well as nanosecond square pulses are experimentally observed in an all-fiber Er-doped fiber laser with 500 kHz low mode-locking repetition rate. The output pulse energy can be greater than 100 nJ at the 560 mW pumping level, indicating the possibility of achieving high pulse energy directly from the laser output. The high energy square pulses output may be useful for practical applications.

1.5 Organization of the thesis

The thesis consists of four chapters. In Chapter 1, the motivation of this research and the overview of mode-locked fiber lasers will be introduced. Chapter 2 is devoted to the principles of mode-locking techniques. Chapter 3 shows the structure of the experiment and the discussion of our results. Finally, Chapter 4 gives the conclusions and future expectations.

Reference

[1.1] H. A. Haus, “Mode-Locking of Lasers,” IEEE J. Selected Topics Quantum Electron. 6, 1173-1185, 2000.

[1.2] W. D. Tan, D. Tang, X. Xu, J. Zhang, C. Xu, F. Xu, L. Zheng, L. Su, and J. Xu, “Passive femtosecond mode-locking and cw laser performance of Yb^{3+}: Sc_2SiO_5,” Opt. Lett. 18, 16739-16744, 2010.

[1.3] J. R. Buckley, S. W. Clark, and F. W. Wise, “Generation of ten-cycle pulses from an ytterbium fiber laser with cubic phase compensation,” Opt. Lett. 31, 1340-1342, 2006.

[1.4] F. Ö. Ilday, T. Sosnowskiand, F. W. Wise, “High-energy femtosecond stretched-pulse fiber laser with a nonlinear optical loop mirror,” Opt. Lett. 27, 1531-1533, 2002.

[1.5] J. Y. Huang, W. C. Huang, W. Z. Zhuang, K. W. Su, Y. F. Chen, and K. F. Huang, “High-pulse-energy, passively *Q*-switched Yb-doped fiber laser with AlGaInAs quantum wells as a saturable absorber,” Opt. Lett. 34, 2360-2362, 2009.

[1.6] F. Röser, T. Eidam, J. Rothhardt, O. Schmidt, D. N. Schimpf, J. Limpert, and A. Tünnermann, “Millijoule pulse energy high repetition rate femtosecond fiber chirped-pulse amplification system,” Opt. Lett. 32, 3495-3497, 2007.

[1.7] S. Kobtsev, S. Kukarin and Y. Fedotov, “Ultra-low repetition rate mode-locked fiber laser with high-energy pulses,” Opt. Express 16, 21936-21941, 2008.

[1.8] X. Tian, M. Tang, X. Cheng, P. P. Shum, Y. Gong and C. Lin, “High-energy wave-breaking-free pulse from all fiber mode-locked laser system,” Opt. Express 17, 7222-7227, 2009.

[1.9] C. Lecaplain, C. Chédot, A. Hideur, B. Ortaç and J. Limpert, “High-power all-normal-dispersion femtosecond pulse generation from a Yb-doped large-mode-area microstructure fiber laser,” Opt. Lett. 32, 3738-3740, 2007.

[1.10] M. Baumgartl, B. Ortaç, C. Lecaplain, A. Hideur, J. Limpert and A.Tünnermann, “Sub-80 fs dissipative soliton large-mode-area fiber laser”, Opt. Lett.35, 2311-2313, 2010.

[1.11] S. H. Cho, F. X. Kärtner, U. Morgner, E. P. Ippen, J. G. Fujimoto, J. E. Cunningham and W. H. Knox, “Generation of 90-nJ pulses with a 4-MHz repetition-rateKerr-lens mode-locked Ti:Al_2O_3 laseroperating with net positive and negative intracavity dispersion,” Opt. Lett.26, 560-562, 2001.

[1.12] L. M. Zhao, D. Y. Tang, T. H. Cheng and C. Lu, “Nanosecond square pulse generation in fiber lasers with normal dispersion,” Optics Communications, 272, 431–434, 2007.

[1.13] X. Wu, D. Y. Tang, H. Zhang and L. M. Zhao, “Dissipative soliton resonance in an all-normal dispersion erbium-doped fiber laser,” Opt. Express 17, 5580-5584, 2009.

[1.14] X. Li, X. Liu, X. Hu, L. Wang, H. Lu, Y. Wang, and W. Zhao, “Long-cavity passively mode-locked fiber ring laser with high-energy rectangular-shape pulses in anomalous dispersion regime,” Opt. Lett. 35, 3249-3251, 2010.

[1.15] D. Mao, X. Liu, L. Wang, H. Lu and L. Duan, “Dual-wavelength step-like pulses in an ultra-large negative-dispersion fiber laser,” Opt. Express 19, 3996-4001, 2011.

[1.16] L. E. Nelson, S. B. Fleischer, G. Lenz, and E. P. Ippen, “Efficient frequency doubling of a femtosecond fiber laser,” Opt. Lett.21, 1759-1761,

1996.

[1.17] N. B. Chichkov, K. Hausmann, D. Wandt, U. Morgner, J. Neumann and D. Kracht, “High-power dissipative solitons from an all-normal dispersion erbium fiber oscillator,” Opt. Lett. 35, 2807-2809, 2010.

[1.18] J.-H. Lin, D. Wang and K.-H. Lin, “High energy pulses generation with giant spectrum bandwidth and sub-megahertz repetition rate from a passively mode-locked Yb-doped fiber laser in all normal dispersion cavity,” Laser Phys. Lett. 8, 66-70, 2011.

[1.19] M. Zhang, L.L. Chen, C. Zhou, Y. Cai, L. Ren, and Z.G. Zhang, “Mode-locked ytterbium-doped linear-cavity fiber laser operated at low repetition rate,” Laser Phys. Lett. 6, 657-660, 2009.

Chapter 2

Principles

2.1 Polarization Additive Pulse Mode-Locking

The additive pulse mode-locking (APM) [2.1] is a common technique for passive mode-locking of lasers. It employs nonlinear Kerr effects in the cavity to attain pulse shortening. The Kerr effects induce different nonlinear phase shifts on the peak and the wings of the pulses. Constructive interference then occurs near the peak of the pulses and destructive interference occurs near the wings. In this way, the pulse-width is shortening. APM is easily achieved in fiber lasers because of the strong nonlinear self-phase modulation (SPM) effects that arise from the small mode field diameter of the fiber.

The particular scheme used in fiber lasers for implementing APM is called the polarization additive pulse mode-locking (P-APM) [2.2]. If the optical pulse in an isotropic optical fiber is with an elliptical polarization state, the nonlinear polarization rotation (NPR) effects will occur for this polarization state due to the nonlinear Kerr effects in the fiber. Fig.2-1 shows the illustration of NPR.

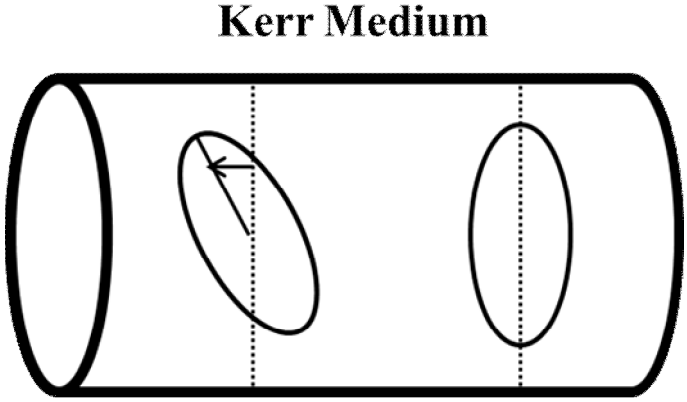

Fig. 2.1 Nonlinear polarization rotation in Kerr medium

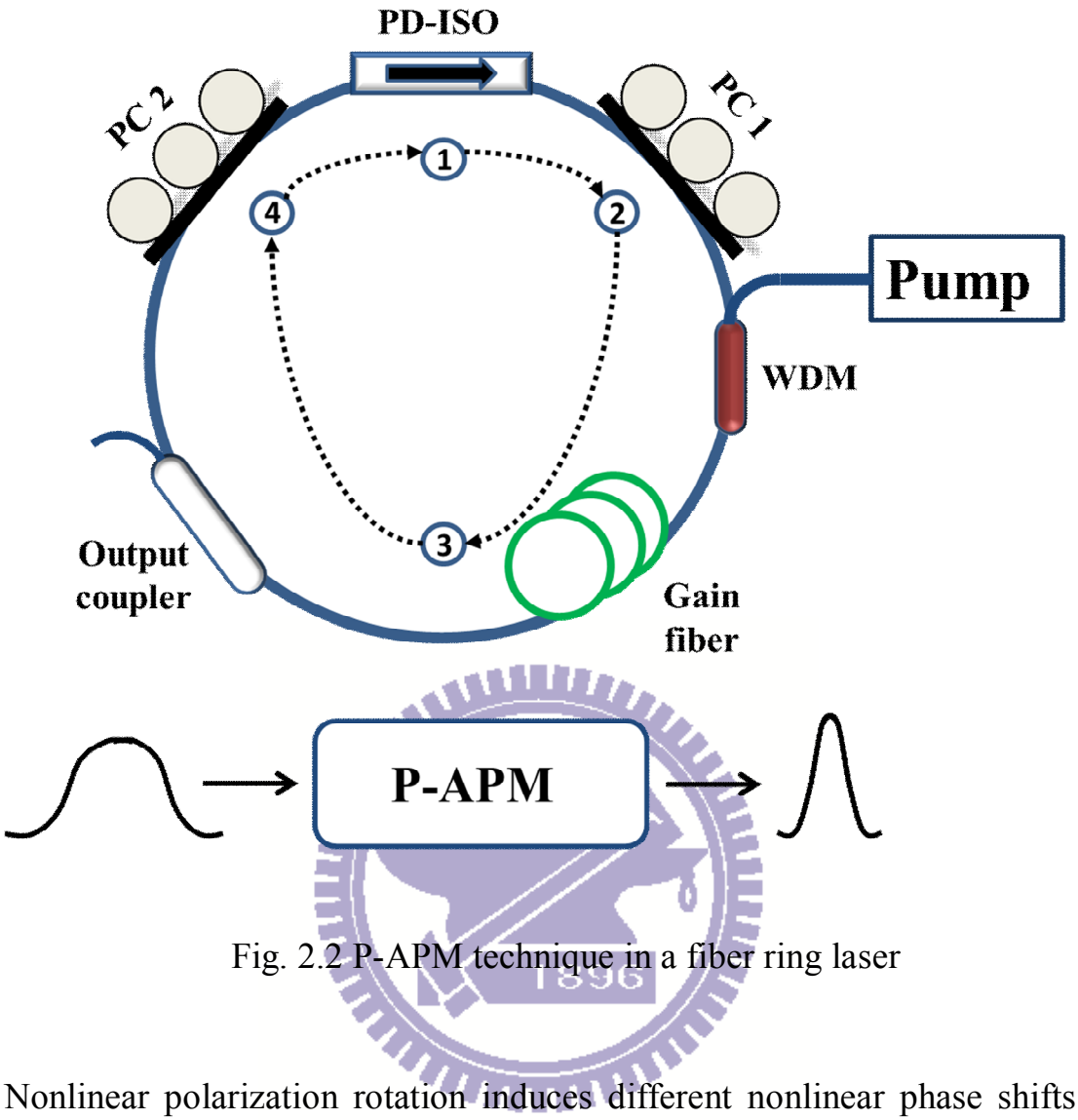

Fig. 2.2 P-APM technique in a fiber ring laser

Nonlinear polarization rotation induces different nonlinear phase shifts on different circular polarization components. The orientation of the polarization is rotated by the nonlinear medium and the quantity of rotation depends on the intensity of the light. Fig. 2.2 shows the schematic of one realization of a fiber ring laser. A polarization dependent isolator (PD-ISO) is for single direction propagation and also serves as a polarizer-analyzer. PC is the inline polarization controller. The following is the principle of the P-APM technique. The light wave is first linearly polarized by the PD-ISO in position ①. Then, the PC1 elliptically polarizes the light wave in position ②.The ellipse can be decomposed into the right- and left-hand circular polarization components.

When the light wave propagates from ② to ③, if the light intensities between two circular components are different, the lightwave experiences different amounts of nonlinear phase shifts for each component. The light polarization orientation starts to rotate, which is known as the nonlinear polarization rotation. Finally, at the position ④ of the ring cavity, the PC2 orients the pulse and selects the lightwave polarized in a particular direction so that the peak of the pulse passes through the analyzer while the wings of the pulse are extinguished. Therefore the ultra-short pulse can be created.

2.2 Nonlinear polarization switching

Nanosecond square pulses can be generated in Er-doped mode-locked fiber laser with a long cavity. It is because the peak power clamping effect [2.3]. Assume a ring laser cavity which includes **L** length of the birefringent element (usually use the birefringent fiber). θ is the azimuth angle of the polarization-dependent isolator with respect to the fast axis and Ω is the rotation angles by polarization controllers. The magnitude of the round trip intensity transmission **T** of the laser system can be express as

$$T = \cos^2 \Omega - \frac{1}{2}\sin(2\theta)\sin[2(\theta - \Omega)] * [1 - \cos 2\pi (L/L_{b0})] \tag{2.2.1}$$

Here $\mathbf{L_{b0}}$ is the natural beat length of the birefringent element. In optical fibers, the beat length at a particular wavelength will change with the input power, which causes the nonlinear polarization switching. Assuming that the pulse is linearly polarized at $\theta = 45^\circ$, the relationship between the new value of

the beat length $\mathbf{L_b}$ and the input power $\boldsymbol{p}$ can be express as

$$L_b / L_{b0} = (\frac{3}{8} + \frac{5}{8}\sqrt{1+p^2})^{-1/2} \tag{2.2.2}$$

where $\boldsymbol{p}$ is the normalized power defined as

$$p = 2n_2 I / 3\Delta n \tag{2.2.3}$$

, **I** is the optical intensity and Δ**n** is the refractive index difference between the fast and the slow axes. The different power-dependent beat length will result in different transmission.

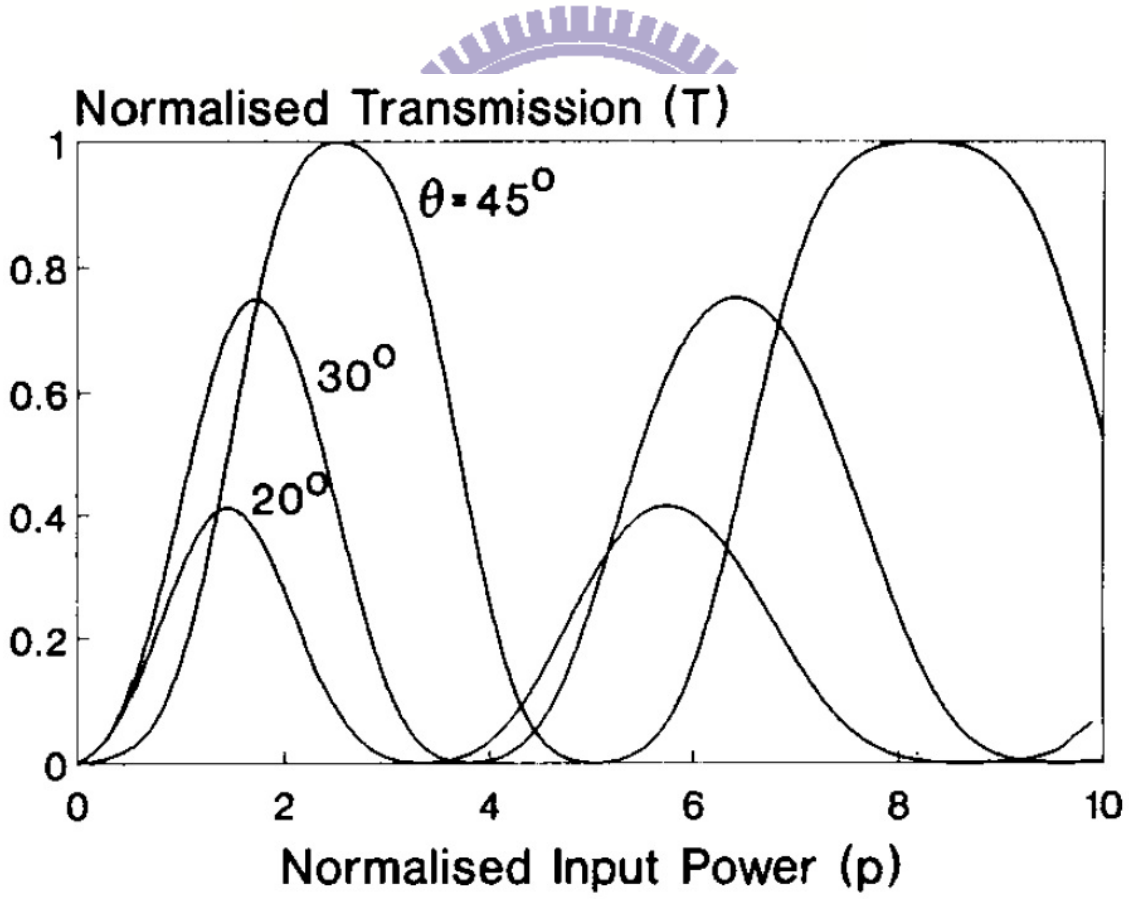

Fig. 2.3 Transmission **T** versus different normalized power $\boldsymbol{p}$ at θ = 45°, 30°, 20° [2.4]

Fig. 2.3 shows the transmission T versus normalized input power ***p*** for linearly polarized light at different θ with Ω being set at 90°. As we can see in the figure, in the small input power region, the transmission is proportional to the input power. However, the transmission will eventually reach a saturation value at a specific power. For example, at $\theta = 45°$, the maximum value of **T** is attained about ***p***= 2.5. As long as the pulse power is sufficient to reach the maximum transmission, the peak power will be clamped due to the transmission saturation. In this case, the mode-locked fiber laser could be operated in the square pulse condition after properly rotating the angles of polarization controllers. In order to have the maximum switching efficiency, we set θ=45° and Ω=90°. According to equations (2.2.1) and (2.2.2), the approximate expression for the lowest normalized power that maximizes the transmission is

$$\frac{2}{2+L_{b0}/L}=\left(\frac{3}{8}+\frac{5}{8}\sqrt{1+p^2}\right) \tag{2.2.3}$$

which can be solved as

$$p_{sw}=\sqrt{\frac{1}{25}\left(2\left(2+L_{b0}/L\right)^2-3\right)^2-1} \tag{2.2.4}$$

Equation (2.2.4) indicates that the switching power is inversely proportion to the fiber length. It means that the square pulses can be generated in the smaller normalized input power if we increase the total cavity length.

2.3 Chirped Gaussian pulses

We consider a simple wave function description for the transform-limited Gaussian pulses, and the incident field as the following form [2.5]

$$A(0,t) = A_0 \exp\left(-t^2/\tau^2\right) \tag{2.3.1}$$

where τ is the pulse-width. In fact, the full width at half maximum (FWHM) pulse-width instead of τ is more commonly used in actual computations. The intensity $\mathbf{I(t) = |A(t)|^2}$ is also a Gaussian function and its FWHM can be expressed as

$$\tau_{FWHM} = (2\ln 2)^{1/2}\,\tau \approx 1.18\tau \tag{2.3.2}$$

This Gaussian pulse has a minimum time-bandwidth product. If the Gaussian pulse has an initial frequency chirp, then equation (2.3.1) will be modified as

$$A(t) = A_0 \exp\left(-t^2/\tau^2\right)\exp\left(jat^2/\tau^2\right) \tag{2.3.3}$$

Where a is a linear chirp parameter. From the equation (2.3.3), the phase φ can be written as

$$\varphi(t) = at^2/\tau^2 \tag{2.3.4}$$

Which is the function of time and $\varphi'' = 2a/\tau^2$. The instantaneous frequency ν_i is given by

$$\upsilon_i = \upsilon_0 + \left(a/\pi\tau^2\right)t \tag{2.3.5}$$

A pulse is said to be chirped if it's instantaneous frequency is time varying. By using equation (2.3.5) one finds that the υ_i is the linear function of time. The

pulse is called up-chirped for $a > 0$, down-chirped for $a < 0$, and unchirped for $a = 0$. To further study how the linear chirp effect on the frequency domain, we perform Fourier transforms for equation (2.3.1), so that

$$A(\upsilon) = \frac{A_0 \tau}{2\sqrt{\pi(1 - ja)}} \exp\left(\frac{\pi^2 \tau^2 \upsilon^2}{1 - ja}\right) \tag{2.3.6}$$

and the spectral intensity $S(\upsilon) = |A(\upsilon)|^2$ is given by

$$S(\upsilon) = \frac{I_0 \tau^2}{4\pi\sqrt{(1 + a^2)}} \exp\left(-\frac{2\pi^2 \tau^2 (\upsilon - \upsilon_0)^2}{1 + a^2}\right) \tag{2.3.7}$$

From equations (2.3.7) and (2.3.2), we set the spectral width at 1/e intensity point and thus the product of FWHM temporal and half-width spectral is given by

$$\tau_{FWHM} \Delta\upsilon = 0.44\sqrt{1 + a^2} \tag{2.3.8}$$

If the chirp $a=0$, the minimum possible time–bandwidth product is obtained for transform-limited pulses. We can use the equation (2.3.8) to find out the chirp parameter in our laser output and try to restore the spectral phase. According to (2.3.6), the spectral phase for a linearly chirped Gaussian pulse is

$$\varphi(\upsilon) = -2\pi^2 \tau^2 \left[1/(1 + a^2)\right] \upsilon^2 \tag{2.3.9}$$

We can also estimate the chirp parameter in the frequency domain. Considering the case of Gaussian form, the incident field of a chirped pulse in frequency domain can be written as

$$F(\omega) = \exp\left[-0.5 * (\alpha - i\delta)\omega^2\right] \tag{2.3.10}$$

Where α is the band-width constant and δ is the frequency chirp parameter. The Fourier transform of the equation (2.3.10) is

$$F(t) = \exp\left[-0.5/(\alpha - i\delta)t^2\right]$$
$$= \exp\left[-0.5*\frac{\alpha}{\alpha^2+\delta^2}t^2 - i0.5*\frac{\delta}{\alpha^2+\delta^2}t^2\right] \quad (2.3.11)$$

Like the previous derivation, the FWHM value both in the time and frequency domains is given by

$$FWHM_\omega = 2\sqrt{\ln 2/\alpha} \quad (2.3.12)$$

and

$$FWHM_t = 2\sqrt{\ln 2 * \frac{\alpha^2+\delta^2}{\alpha}} \quad (2.3.13)$$

With equations (2.3.12) and (2.3.13), we can utilize the time-width and the optical band-width measured from experiments to estimate the values of α and δ.

Next, we consider the high order chirp term and the equation (2.3.10) will be modified as

$$F(\omega) = \exp\left[-0.5*(\alpha - i\delta - i\gamma\omega)\omega^2\right] \quad (2.3.14)$$

where γ is the third order chirp. It can be estimated by using the filter to scan the whole spectrum and record the corresponding time width. The relationship between central-frequency-difference ($\Delta\lambda$) and filtering time width ($FWHM_t[\Delta\lambda]$) is

$$FWHM_t[\Delta\lambda] = 2\sqrt{\ln 2}\left(\delta - 6\pi c/\lambda^2\,\gamma\Delta\lambda\right)\Big/\sqrt{\alpha'} \quad (2.3.15)$$

where λ is the central wavelength and α' is the filtering bandwidth. Therefore, the characteristic parameters of the laser output pulses can be effectively estimated.

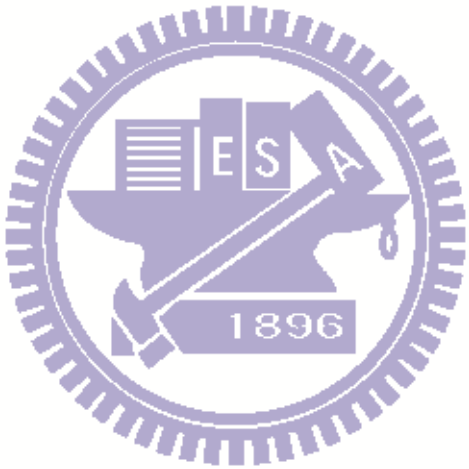

Reference

[2.1] H. A. Haus, J. G. Fujimoto, and E. P. Ippen, “Structures for additive pulse mode locking,” J. Opt. Soc. Am. B 8, 2068-2076, 1991.

[2.2] H. A. Haus, and E. P. Ippen, “Modelocked Fiber Ring Lasers,” OSATOPS on Ultrafast Electronics and Optoelectronics 13, 6-12, 1997

[2.3] Y. Li, X. Gu, M. Yan, E Wu, and H Zeng, “Square nanosecond mode-locked Er-fiber laser synchronized to a picosecond Yb-fiber laser,” Opt. Express 17, 4526-4532, 2009.

[2.4] V. J. Matsas, T. P. Newson, and M. N. Zervas, “Self-starting passively mode-locked fiber ring laser exploiting nonlinear polarization switching,” Opt. Communications 92, 61-66, 1992.

[2.5] B. E. A. Saleh, and M. C. Teich, “Fundamentals of photonics,” second edition, John Wiley &Sons, New Jersey, 2007.

Chapter 3

Experimental setup and results

3.1 Experimental setup

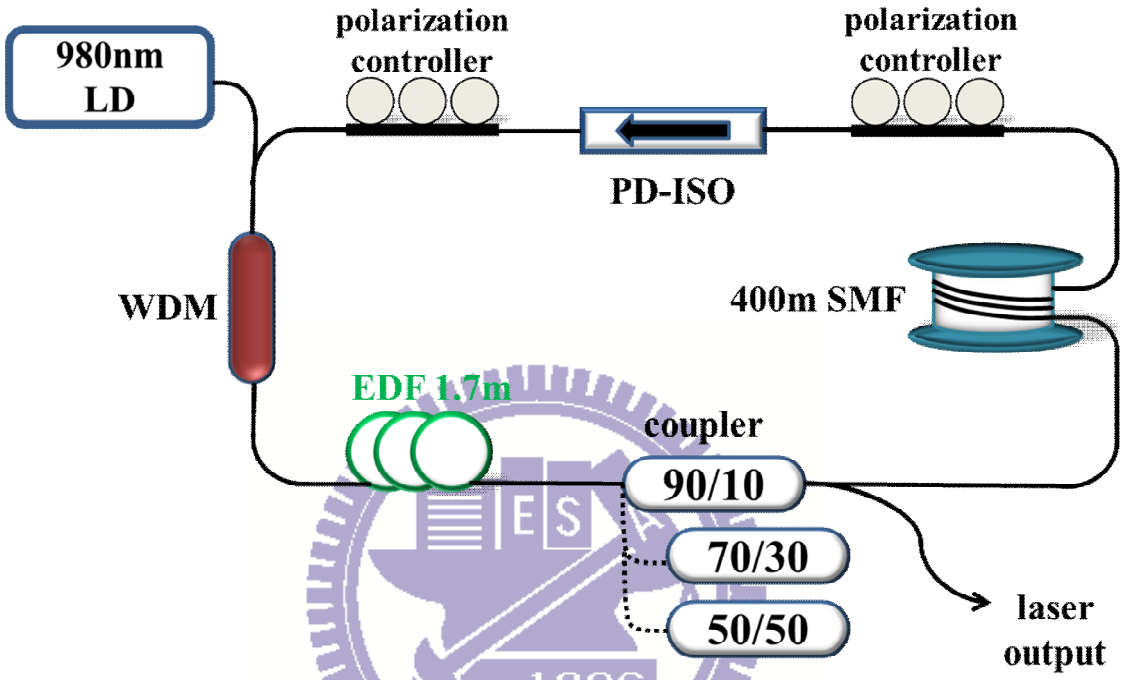

Fig. 3.1 Experimental fiber laser setup

The schematic setup of the all-fiber ring laser in our experiments is shown in Fig. 3.1. The laser is pumped by a 980 nm laser diode through a wavelength-division-multiplexing (WDM) coupler. An Erbium doped fiber of 1.7 m (dispersion 0.05164 ps^2/m) is used as the gain medium. Two polarization controllers (PCs) are employed to adjust the polarization states of the circulating light in the cavity. With the two polarization controllers and the polarization dependent isolator (PD-ISO), the nonlinear polarization evolution mechanism of passive mode-locking is achieved. The 400m long signal mode fiber is added inside laser cavity to provide large nonlinearity for achieving mode-locking and reducing the pulse repetition rate to increase pulse energy. The net cavity

dispersion of the ring laser is estimated to -9.23 ps^2, implying that the laser is operated in a large anomalous dispersion region. In order to attain the highest pulse energy, we change the output coupling ratio (90/10, 70/30, 50/50, 30/70) to observe the change of output power and characterization of mode-locked (ML) pulses. Finally, we use the optical spectrum analyzer (Agilent 86146B), Rf-spectrum analyzer (HP-8591E), power meter (Newport inc.), and high-resolution digital storage oscilloscope (Agilent 86105A 20 GHz) to characterize the laser output pulses.

3.2 Results and discussions

There are many methods to attain the high pulse energy, including to increase the pump power, to reduce the pulse repetition rate as the cavity length increase, and to change the output coupling ratio, etc. In our experiment, the maximum pumping power is about 561mW, and the pulse repetition rate is 500 kHz as we have put 400 m long SMF inside the cavity. We adjust the output coupling ratio to obtain the highest pulse energy. When the pumping power is above a certain threshold, a relatively stable continuous-wave mode-locking (CW-ML) state without pulse breaking can be achieved by properly rotating the paddles of the polarization controllers. Depending on the adjustments of the polarization controllers, either a multi-pulse operation (harmonic mode-locking) or single-pulse regime can be started. Our task is to find the highest output power within the single-pulse operation as much as possible.

Fig. 3.2 shows the RF spectrum of the mode-locked pulse train. Due to the long cavity length, the pulse repetition rate is as low as 500kHz. The corresponding time trace of ML pulse trains measured by the real-time

oscilloscope is shown in Fig.3.3. It can be seen that the time interval of pulse separation is about 2μs. The mode-locked pulse train is relatively stable as also can be seen from the time trace data.

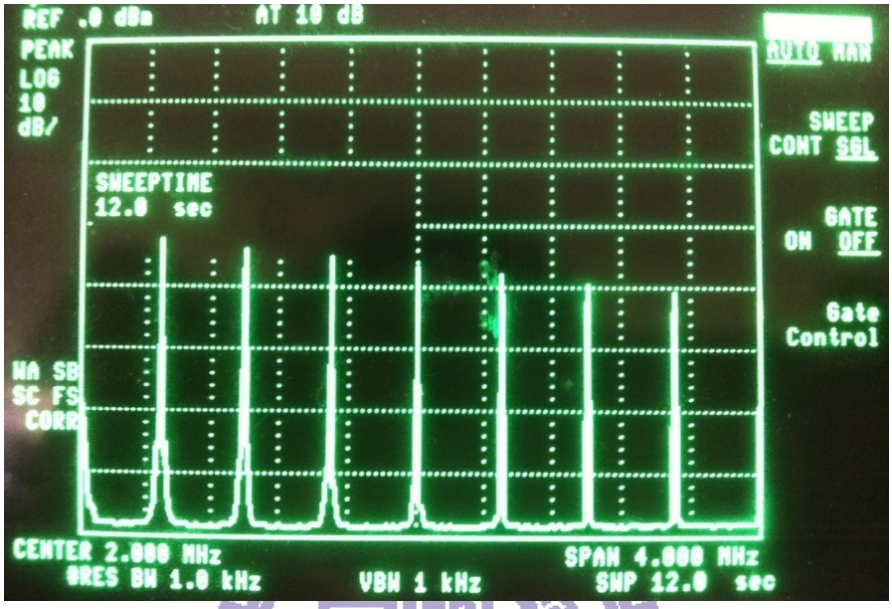

Fig. 3.2 RF spectrum of the pulse train

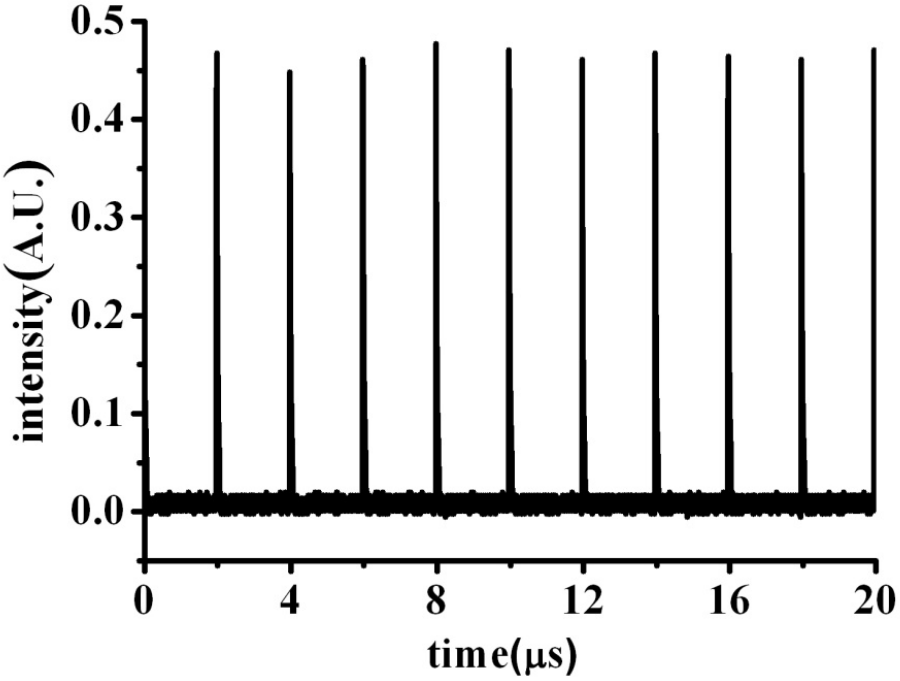

Fig. 3.3 Time trace of the pulse train

3.2-1 High pulse energy

The measured average output powers (left side) and the estimated pulse energy (right side) versus the pump power is illustrated in Fig. 3.4. Using a 90/10 output coupler, the maximum pulse energy is estimated to be about 22.4nJ at the 570mW pumping level with the 500 kHz repetition rate and 11.2mW average output power. It should still be possible to further increase the pulse energy by optimizing the cavity design, so we keep trying different coupling ratios.

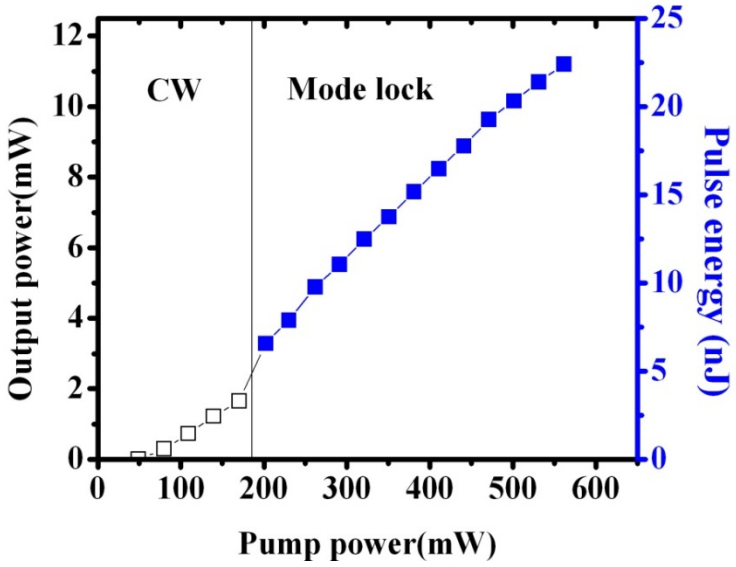

Fig. 3.4 Pulse energy and output power versus pump power with 90/10output coupler

As illustrated in Fig. 3.5, the corresponding pulse energy is increased to be about 63.2 nJ using the 70/30 output coupler because the maximum output power is increased to be 31.6mW. The threshold pump power for mode-locking is about 225mW. The pulse energy and average output power still grows linearly with the pump power, indicating that even higher pulse energies can be expected.

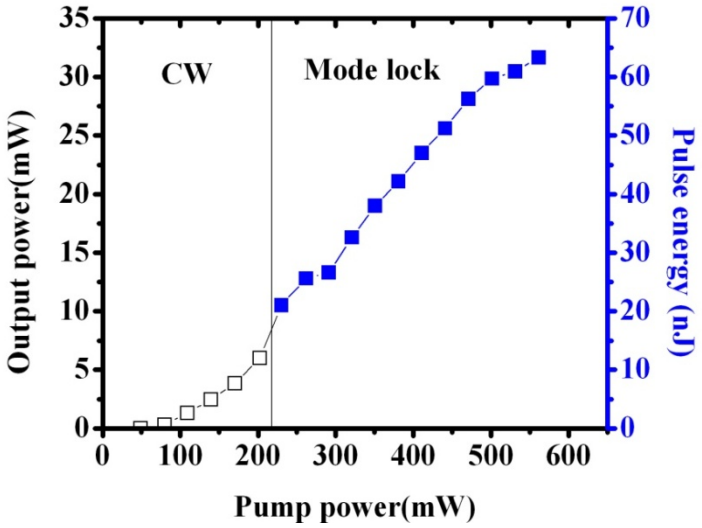

Fig. 3.5 Pulse energy and output power versus pump power with 70/30output coupler

After increasing the output coupling ratio to be 50%, the output light intensity is equal to that storage inside the laser cavity. The pulse energy and average output power versus the pumping power are illustrated as shown in Fig. 3.6(b). The threshold pump power for mode-locking is raised to 320mW and the maximum output pulse energy is over 100 nJ. After proper rotating the PCs, we can observe the mode-locked pulses with relatively wide optical spectrum bandwidth as illustrated in Fig. 3.6(a). The center wavelength is about 1585 nm and the 3dB bandwidth is 50 nm. A broad optical spectrum bandwidth indicates that ultra-short pulses can be generated through proper external compression mechanism. After properly rotating the angles of the polarization controllers, the relative narrower spectral bandwidth about 10nm can be produced as shown in Fig. 3.7(a). Fig. 3.7(b) shows that the highest output power and pulse energy are 63 mW and 126 nJ, respectively. This indicates that the narrower spectral bandwidth case can reach higher pulse energy.

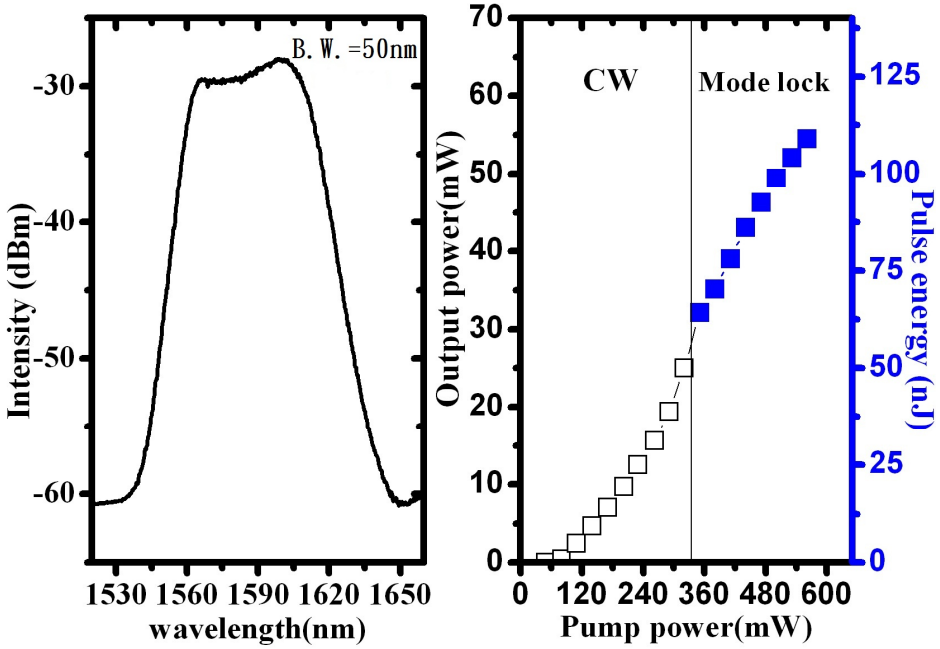

Fig. 3.6(a) Optical spectrum with broaden bandwidth (b)corresponding pulse energy and output power by increasing the pump power (with 50/50 coupler)

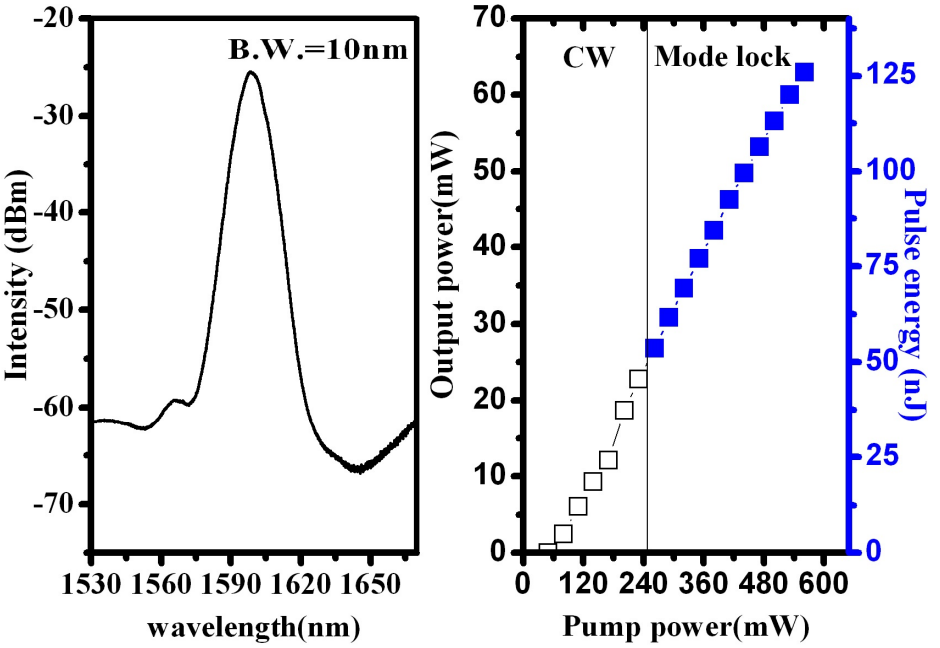

Fig. 3.7(a) Optical spectrum with narrow bandwidth (b)corresponding pulse energy and output power versus pump power (with 50/50 coupler)

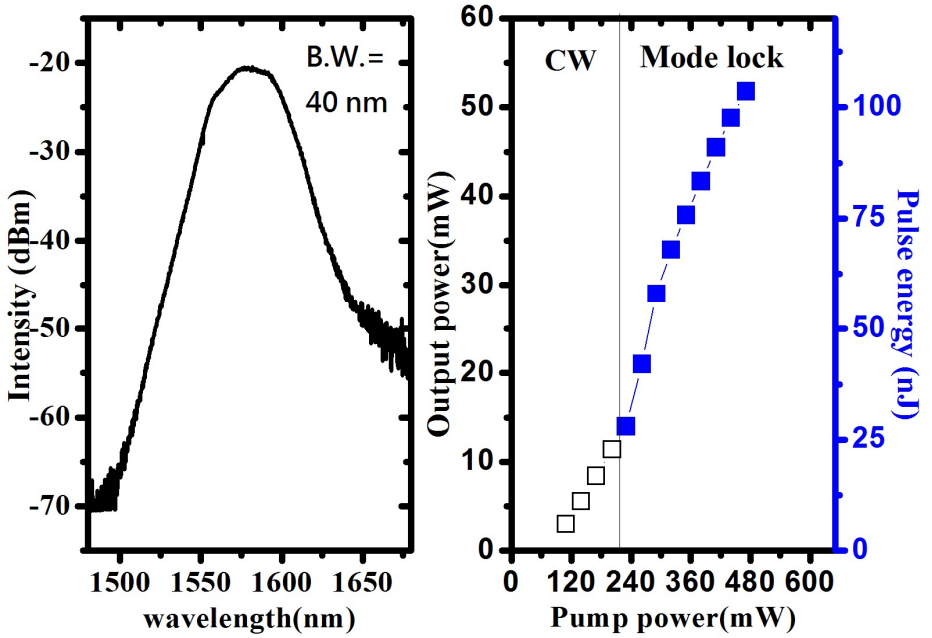

Fig. 3.8(a) Optical spectrum with broaden bandwidth (b)corresponding pulse energy and output power by increasing the pump power (with 30/70 coupler)

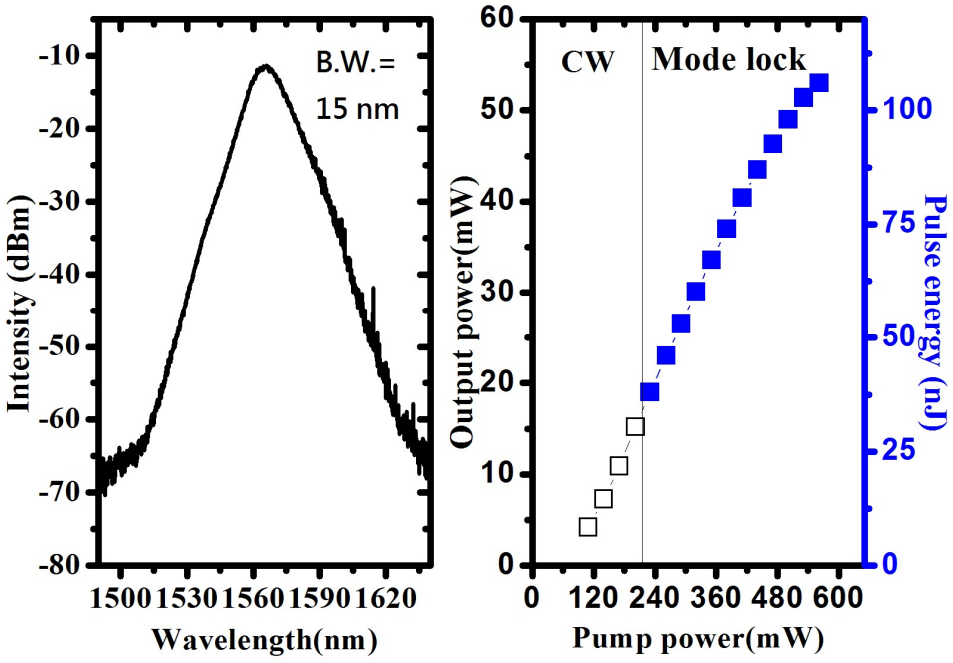

Fig. 3.9(a) Optical spectrum with narrow bandwidth (b)corresponding pulse energy and output power versus pump power (with 30/70 coupler)

In order to further increase the pulse energy, we use a 30/70 output coupler in which 30% of the light is feedback into the cavity and 70% of the light is output. The reduction of pumping power in the cavity makes it more difficult to produce the mode-locking state. The measured pulse energies versus the pump powers are shown in Fig. 3.8 and Fig. 3.9. As we can see, the pulse energy cannot exceed 106nJ whether the optical spectrum bandwidth of ML pulses are broaden (40 nm) or narrow (15 nm). Figure 3.10 shows the maximum pulse energy at the 560 mW pump power using different output coupling ratios. The 50/50 coupling ratio maintains a stable mode-locking state without pulse breaking and attains the highest pulse energy about 126 nJ.

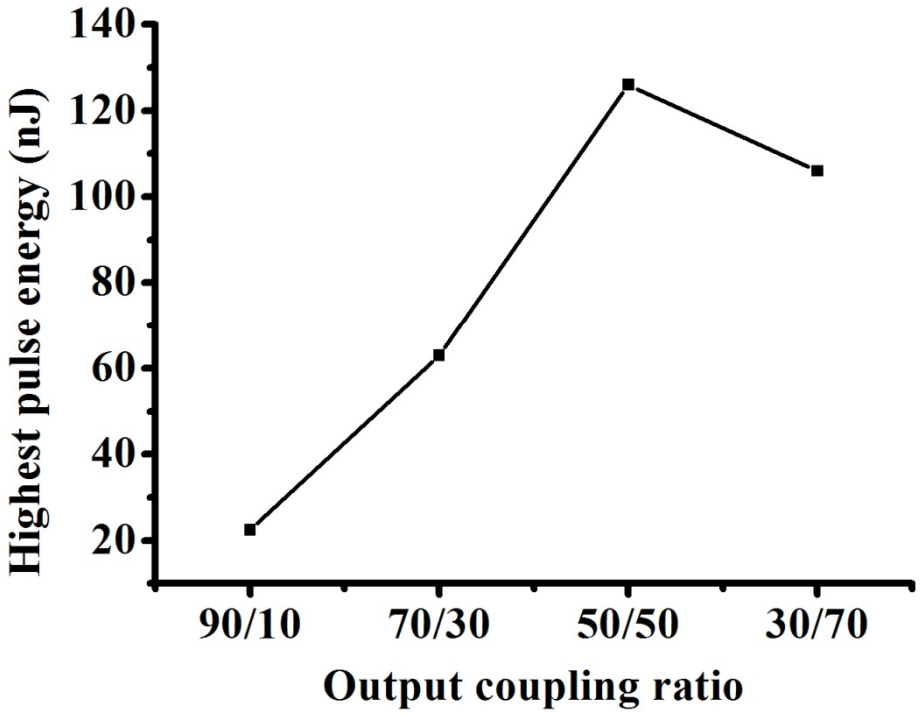

Fig. 3.10 Output coupling ratio versus pulse energy

3.2-2 Square pulse

By carefully adjusting the polarization controllers, a stable ML pulses with square shape are also observed. Fig. 3.11 shows the expanded single pulse trains measured from the high revolution oscilloscope at different pump powers with 50/50 output coupler. Unlike the previous results, the pulse maintains a stable square-like shape without pulse breaking. The 3 dB duration of square pulse increases with the pump strength, while the highest amplitude of the pulse almost remains constant as the pump power variation. Fig. 3.12 indicates the corresponding optical spectra of ML pulses with square shape at lower (solid) and higher (dash) pump powers. The center wavelength is located about 1569 nm and the 3dB bandwidth maintains a constant at different pump power.

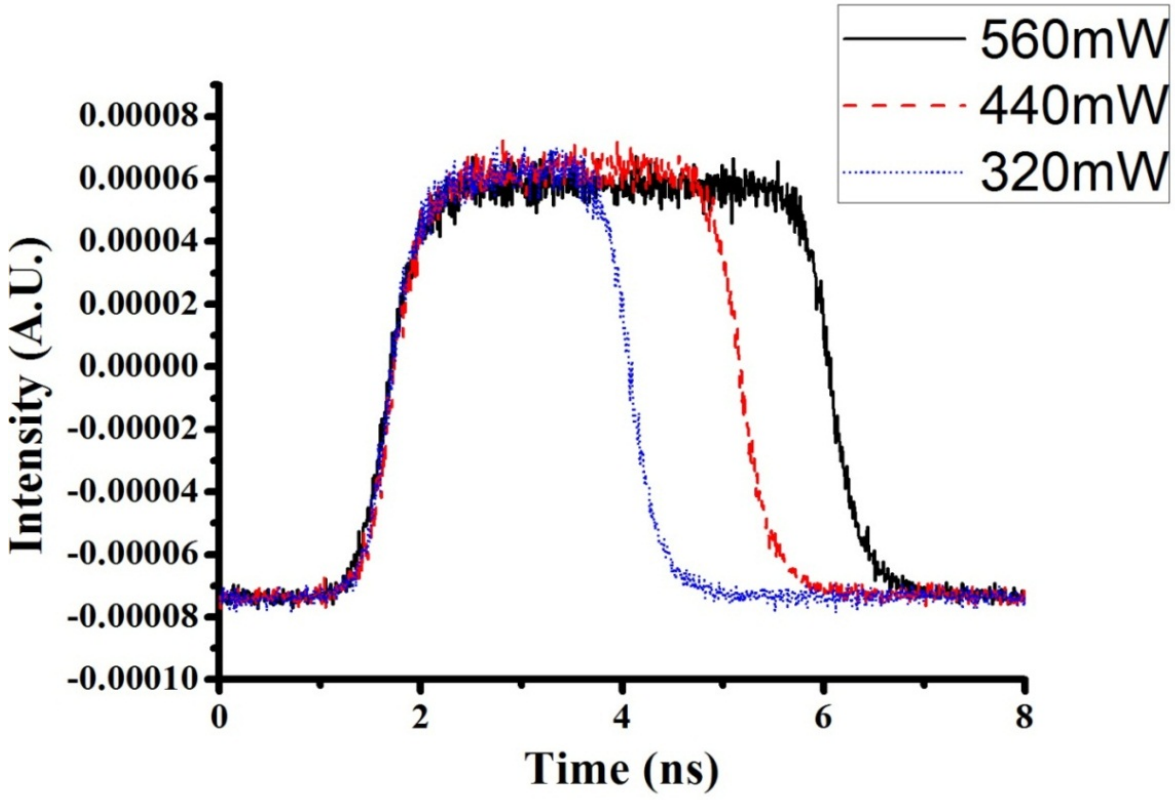

Fig. 3.11 Expanded single pulse traces under different pump power (With50/50 coupler)

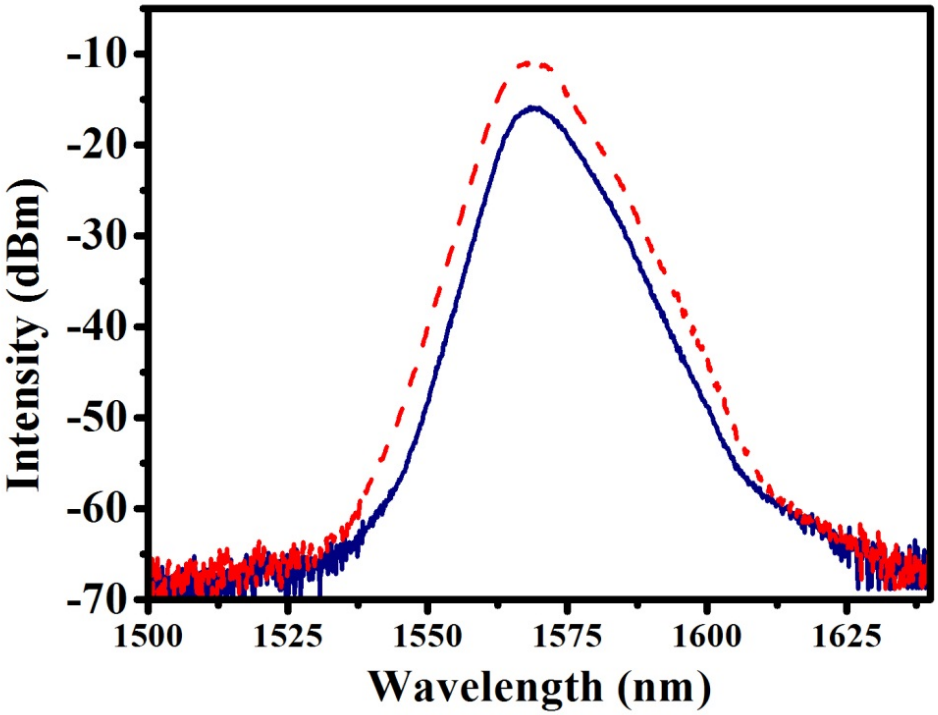

Fig. 3.12 Optical spectra of the square pulses

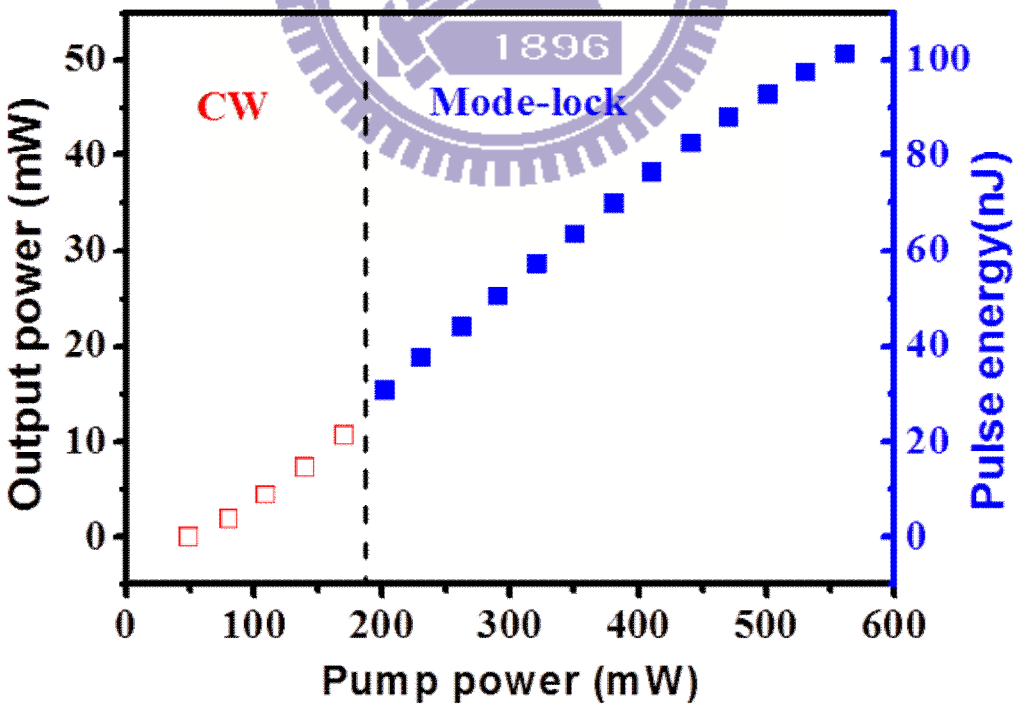

Fig. 3.13 Pulse energy and output power versus pump power

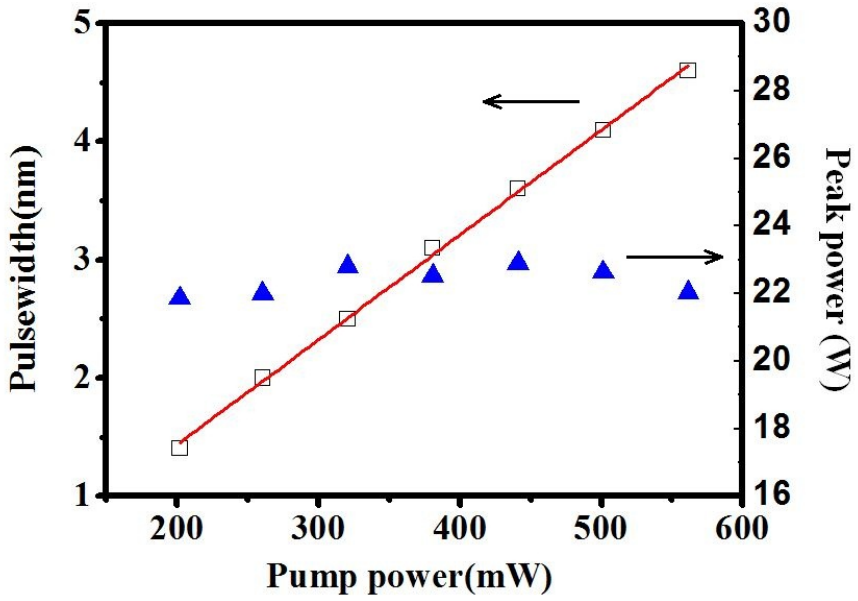

Fig. 3.14 Pulse energy and output power versus pump power (With 50/50 coupler)

Under the square pulse condition, the threshold pump power for stable mode-locked pulses generation is about 200 mW as shown in Fig.3.13. The maximum pulse energy and output power is 100 nJ and 50 mW under the 560 mW pumping power level. Fig. 3.14 indicates that the square pulse-width versus the pumping power grows linearly and the maximum 3 dB duration of square pulse is 4.6 ns, which is limited by the pump power injected into the cavity. Based on the measured pulse parameters, we estimate that the peak power of the square pulse output was about 22 W at different pump powers. The square shape pulse can also be experimentally obtained by using a 70/30 output coupler. Through proper adjusting the polarization state by the PCs and keeping the pumping at the 560 mW, the short pulse-width about 2.4 ns and highest pulse energy about 100 nJ can be experimentally obtained to achieved the highest peak power about 44 W as shown in Fig. 3.15.

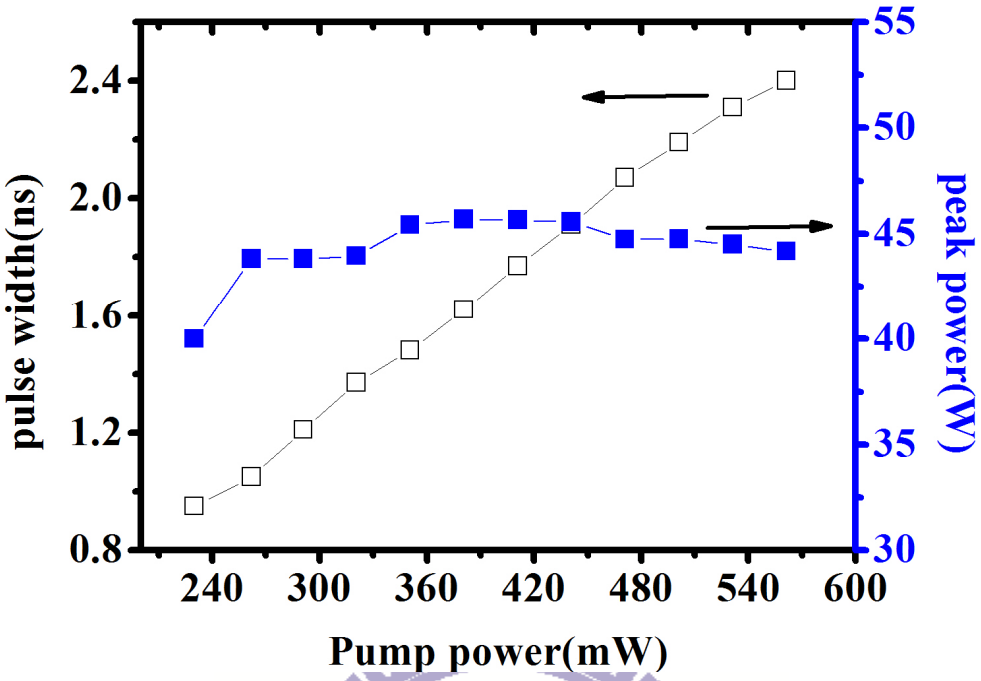

Fig. 3.15 Pulse energy and output power versus pump power

(With 30/70 coupler)

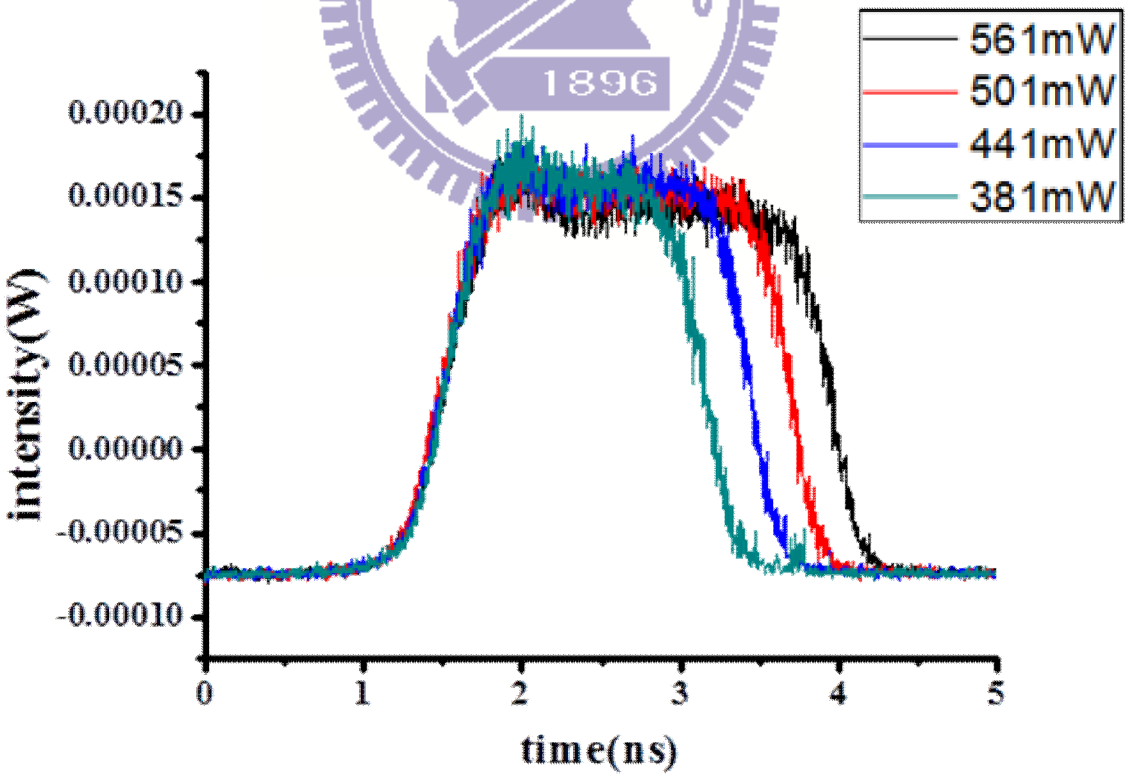

Fig. 3.16 Expanded single pulse traces under different pump power

(With 30/70 coupler)

The expanded single pulse trains generated from our laser with a 30/70 coupler are shown in Fig. 3.16. Like the previous results, the nanosecond square pulses can still be maintained as the pump power varies.

It is interesting to find that the center wavelength can be fine-tuned through PCs at the same pump power. The center wavelength can be effectively tuned from 1565 nm to 1600 nm by properly rotating the PCs as shown in Fig. 3.17. At the short wavelength region, the 3dB bandwidth is about 10 nm. The obtained spectrum bandwidth will become broadened at the longer wavelengths. However, the relatively narrow bandwidth appears again when the center wavelength approaches 1600 nm. Table 3.1 shows the different center wavelength versus the bandwidth.

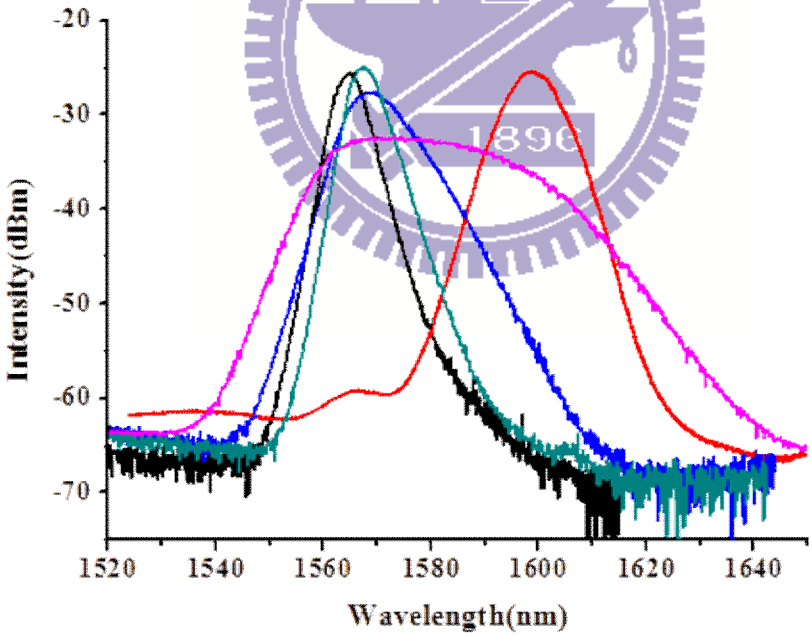

Fig. 3.17 Tenability of the center wavelength

Center wavelength (nm)	1564	1567	1568	1580	1598
Bandwidth (nm)	5	6	11	35	9

Table. 3.1 Different center wavelength versus bandwidth

In our fiber laser, there are many different operation states that can be obtained with different polarization controller settings and intra-cavity peak powers. The operation state with broader bandwidth can more easily break to result in multiple pulse operation or harmonic mode locking [3.1]. The laser output power as a function of increasing pump power with different laser operation regimes is shown in Fig. 3.18. The laser operates at a stable fundamental mode-locking state as pump power above 200mW. The optical spectrum and the time trace of pulse trains are illustrated in Fig. 3.19 and Fig. 3.20. It can be seen that the center wavelength is about 1580 nm and the 3dB spectrum bandwidth is 38 nm. The time interval of pulse separation is about 2μs, corresponding to 500kHz repetition rate. The pulses maintained stable operation until 400mW pump power, and the obtained pulse energies are between 35 to 75 nJ.

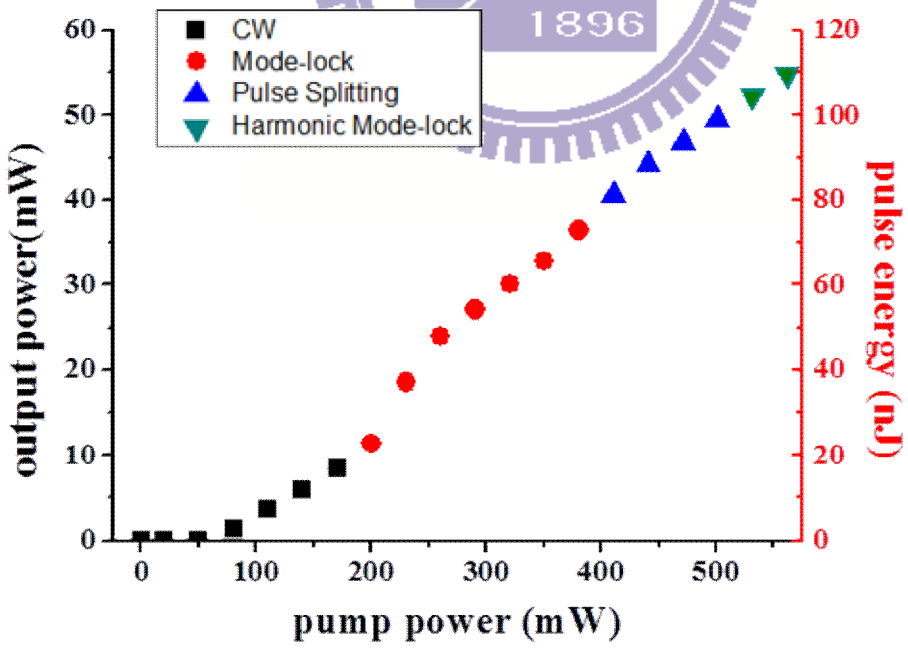

Fig. 3.18 Pulse energy and output power versus pump power with different laser operation regimes indicated

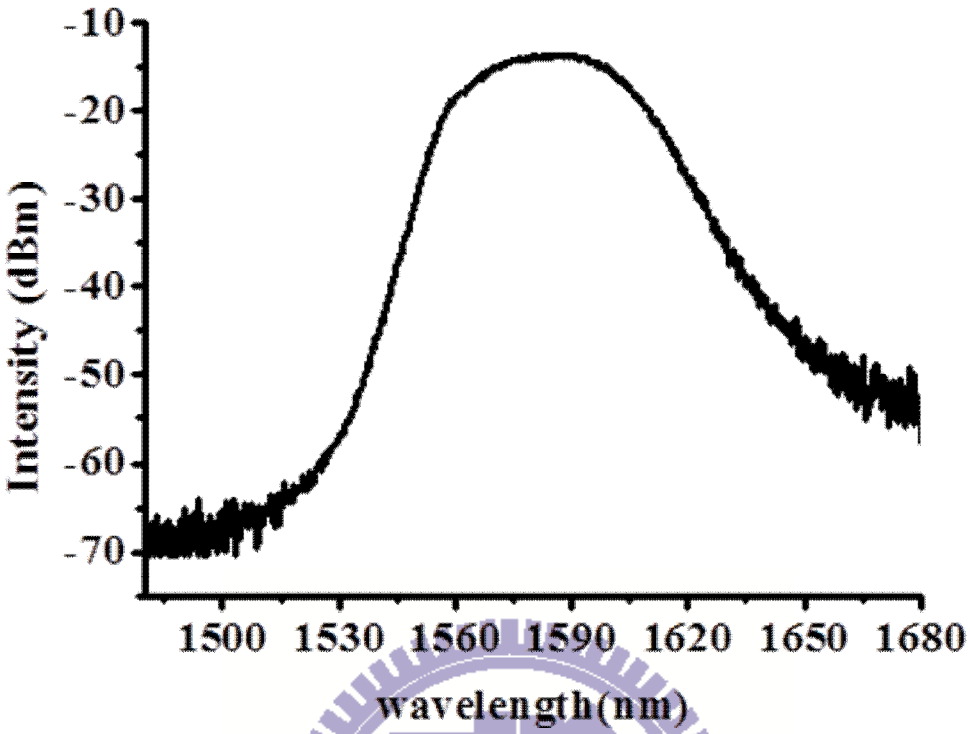

Fig. 3.19 Optical spectrum in mode-locking state

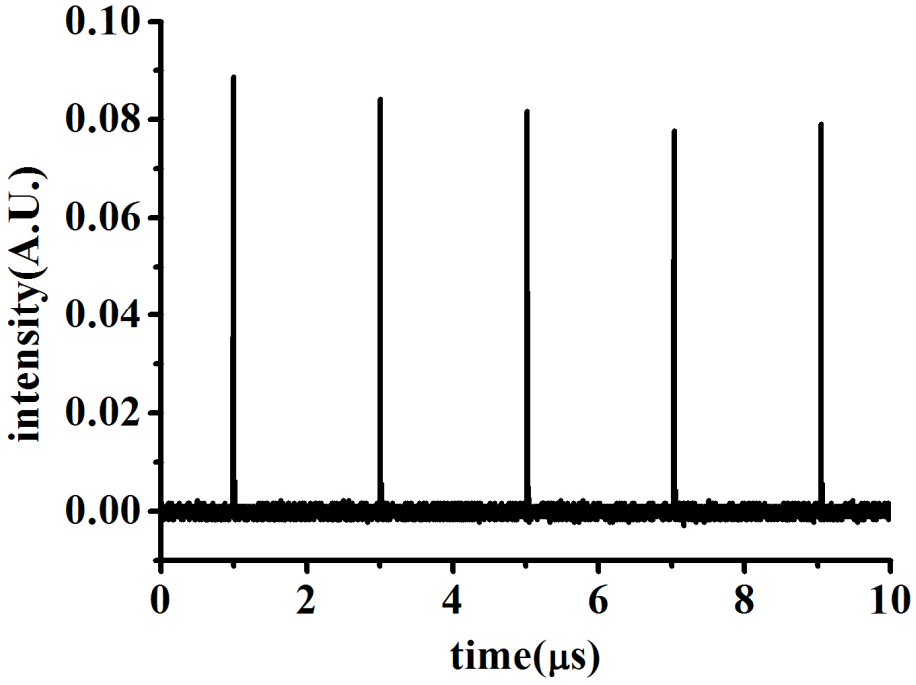

Fig. 3.20 Time trace of the pulse train in mode-locking state

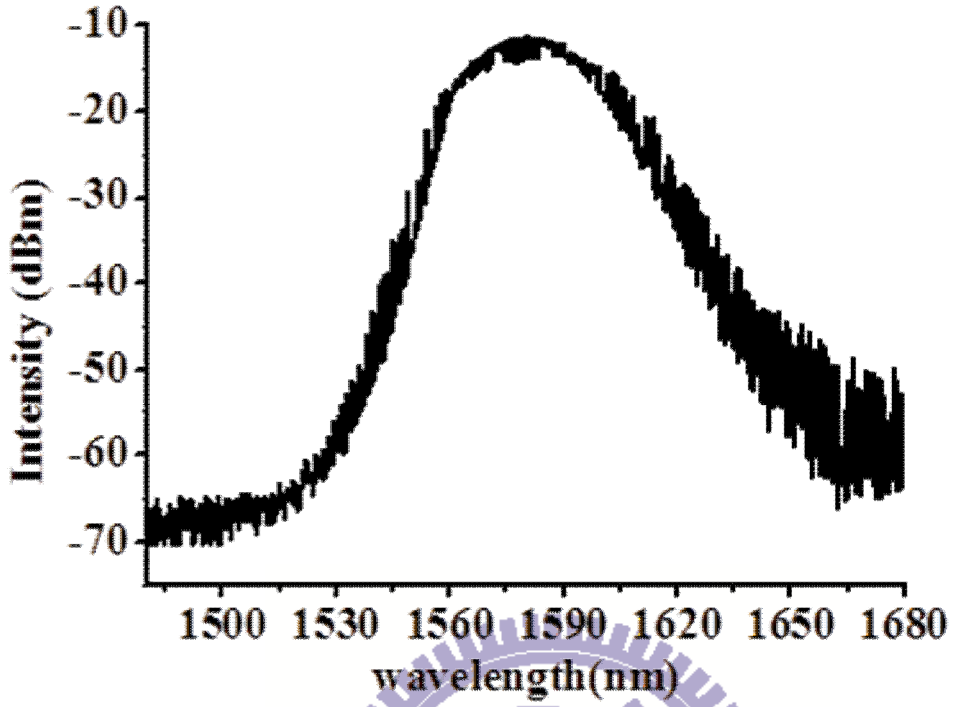

Fig. 3.21 Unstable Optical spectrum in pulse splitting state

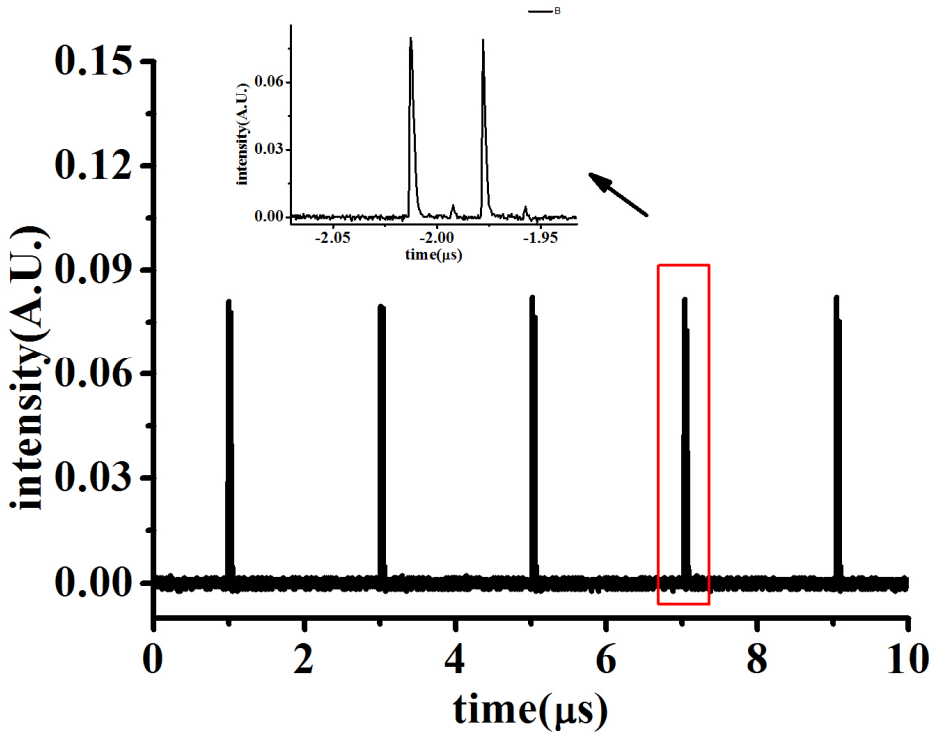

Fig. 3.22 Time trace of the pulse train in pulse splitting state

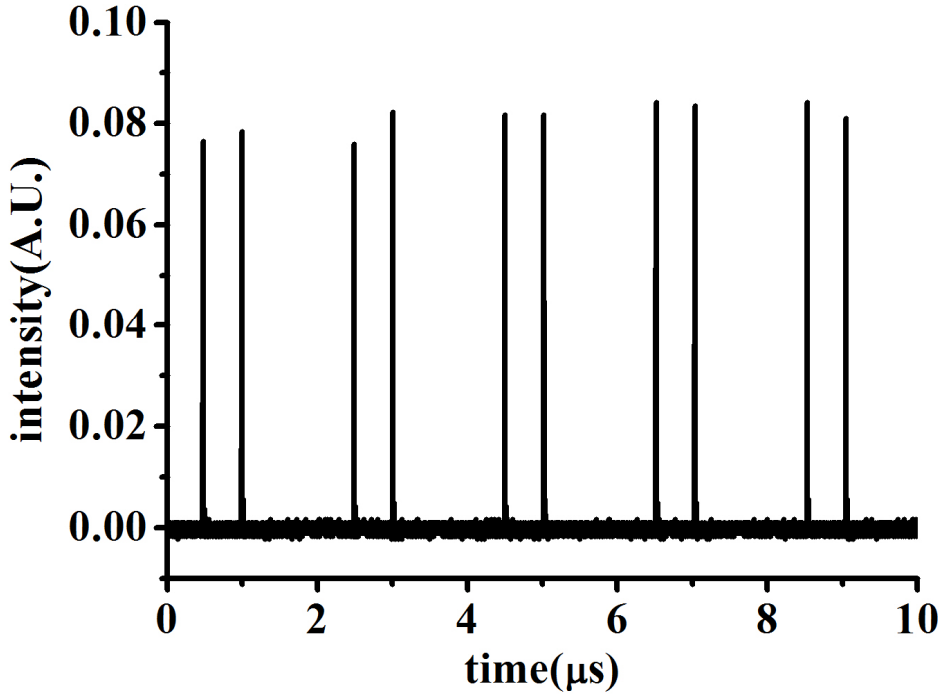

Fig. 3.23 Time trace of the uncontrolled splitting pulses

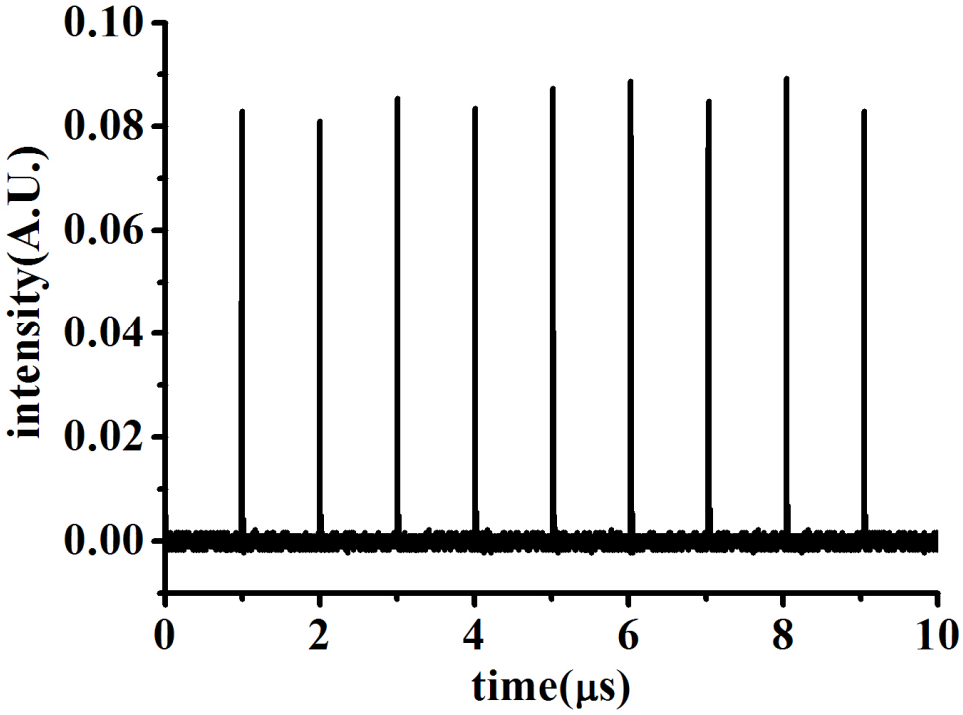

Fig. 3.24 Time trace of the pulse train in harmonic mode-locking state

As the pump power is above 400mW, the mode-locked pulses will break up into multiple pulses and the optical spectrum becomes noisy. Fig. 3.21 and Fig. 3.22 show the obtained spectrum and pulse train in the pulse splitting state. This is because the maximum sustained energy of single pulse is limited and the pulses will break as the pumping power increase [3.2]. The splitting pulses are uncontrolled as shown in Fig. 3.23 until the pumping power is increased about 520mW. Harmonic mode-locking state is observed as illustrated in Fig. 3.24 and the repetition rate is thus increased to 1MHz. Fig. 3.25 shows the optical spectrum in harmonic mode-locking state.

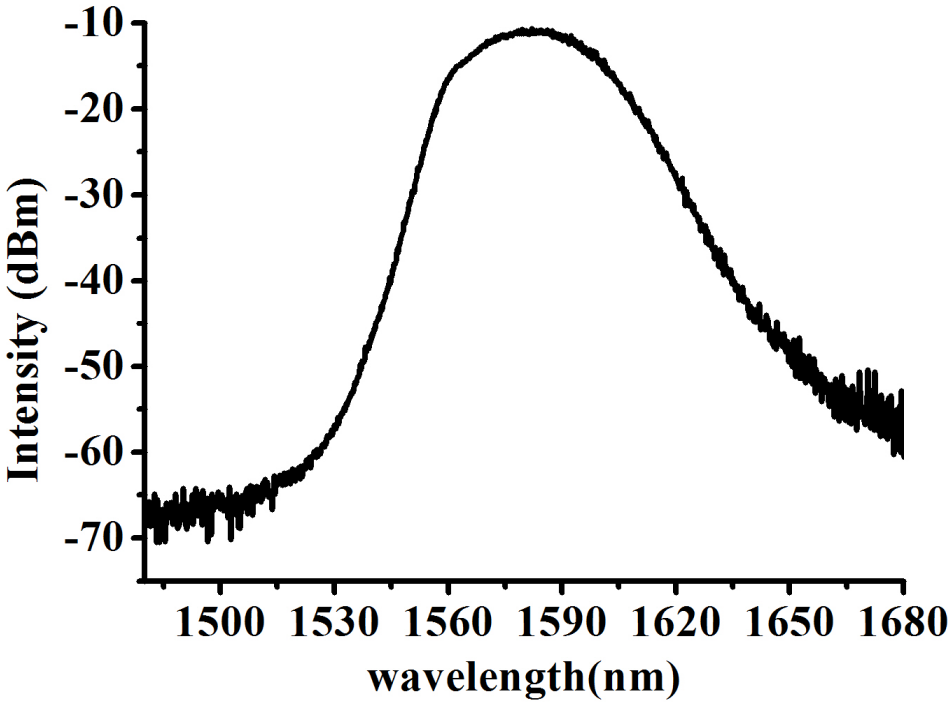

Fig. 3.25 Optical spectrum in harmonic mode-locking state

3.2-3 Chirped pulse

From section 3.2 we demonstrate a novel passive mode-locked all-fiber Er-doped fiber laser with the highest pulse energy over 100 nJ. In this section, we want to characterize the chirp properties of our laser outputs for further compressing the pulse-width by an external pulse compression section to obtain the ultra-short pulses with higher peak power. In the beginning, we operate the laser to be with a relatively flat optical output spectrum. Fig. 3.24 and Fig 3.25 show the original optical spectrum and time trace of single pulse. The center wavelength is about 1570 nm and the 3dB spectrum bandwidth is 30 nm. At 411 mW pumping power, the pulse-width measured from high-resolution digital storage oscilloscope is about 350 ps. In section 2.3 we know that the parameter α and δ can be acquired by the pulse-width and the 3dB spectrum bandwidth. To determine the nonlinear chirp parameter γ, we use a tunable optical filter to select one strip of the optical spectrum from the ML pulses and measure the corresponding pulse-width. In the beginning, we filter out more than half of optical spectrum range and keep only the center part. The center wavelength of optical spectrum is 1569 nm and the spectrum bandwidth is 3 nm as shown in Fig. 3.26. Next, we keep the filtering bandwidth about 3nm and shift the center wavelength from the short edge to the long edge every 9 nm as shown in Fig.3.28 and Fig. 3.30. The filtered pulse shapes measured from the high revolution digital oscilloscope are shown in Fig. 3.27, Fig.3.29 and Fig.3.31. We use these measured pulse-width and spectral bandwidth for nonlinear chirp estimation.

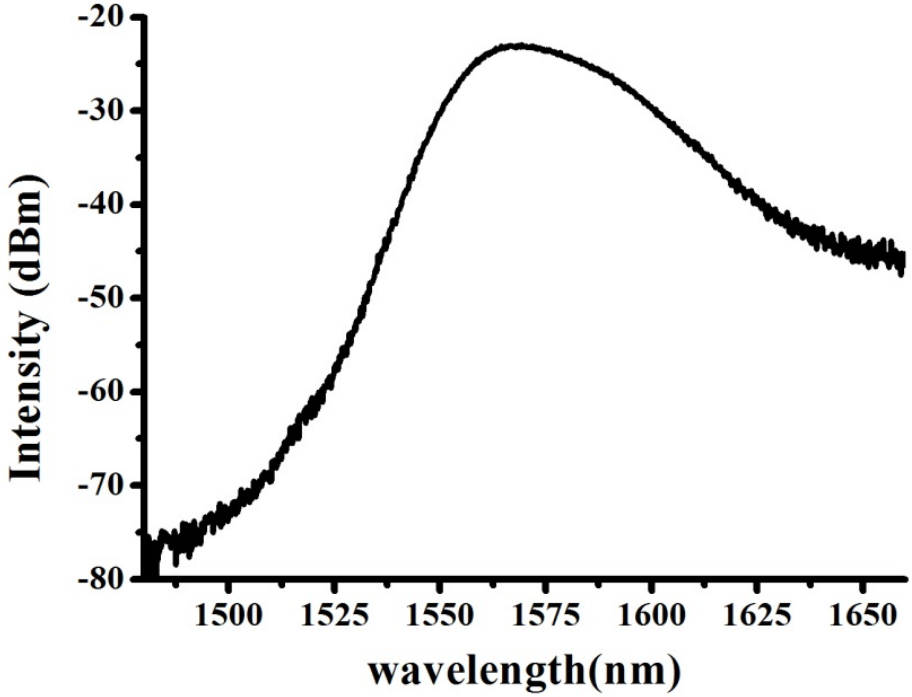

Fig. 3.26 Optical spectrum before filtering

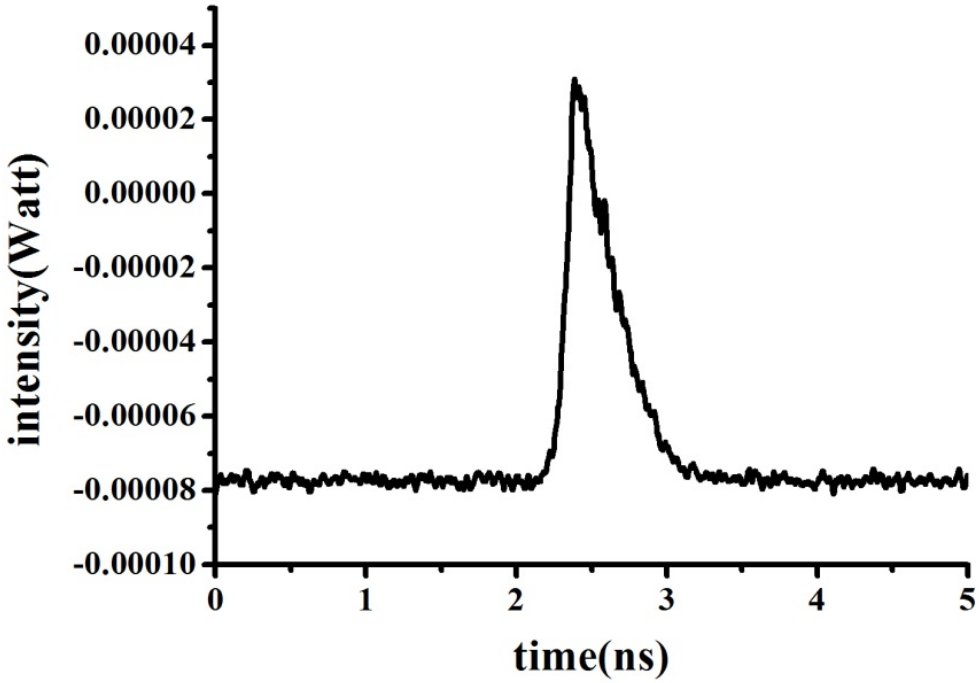

Fig. 3.27 Time trace of single pulse

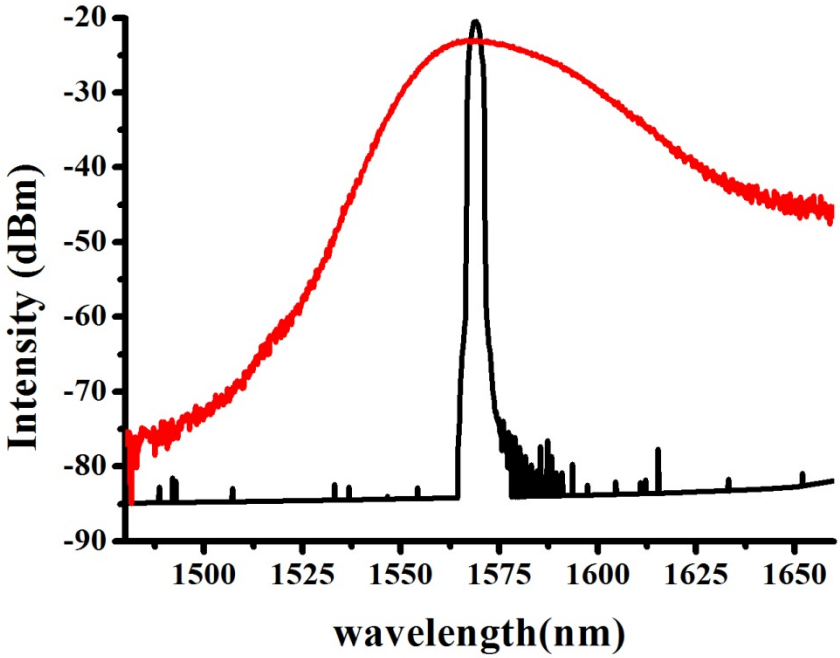

Fig. 3.28 Optical spectrum before (up) and after (down) filtering.

(middle remain)

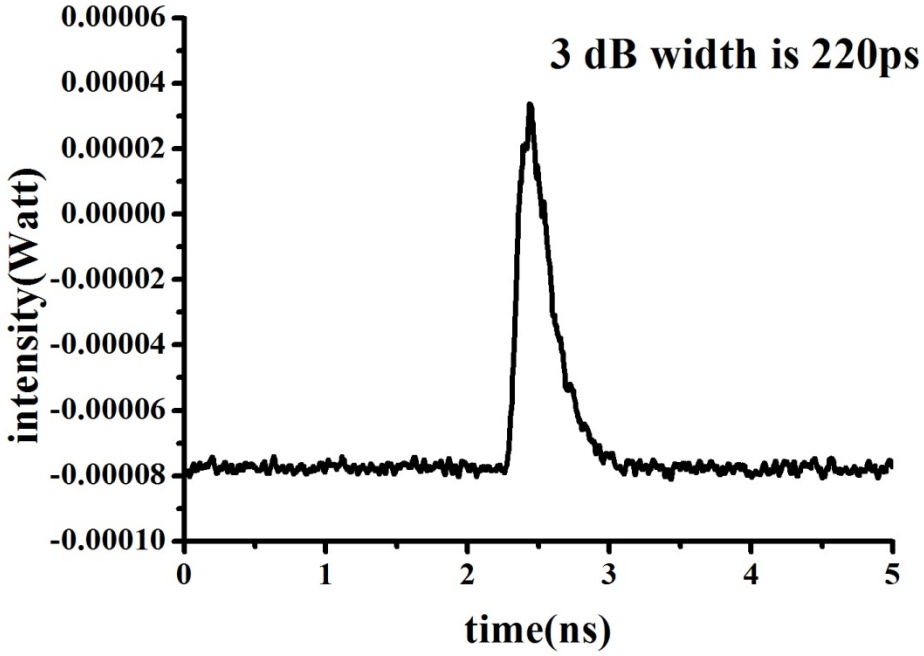

Fig. 3.29 Time trace of single pulse

(middle remain)

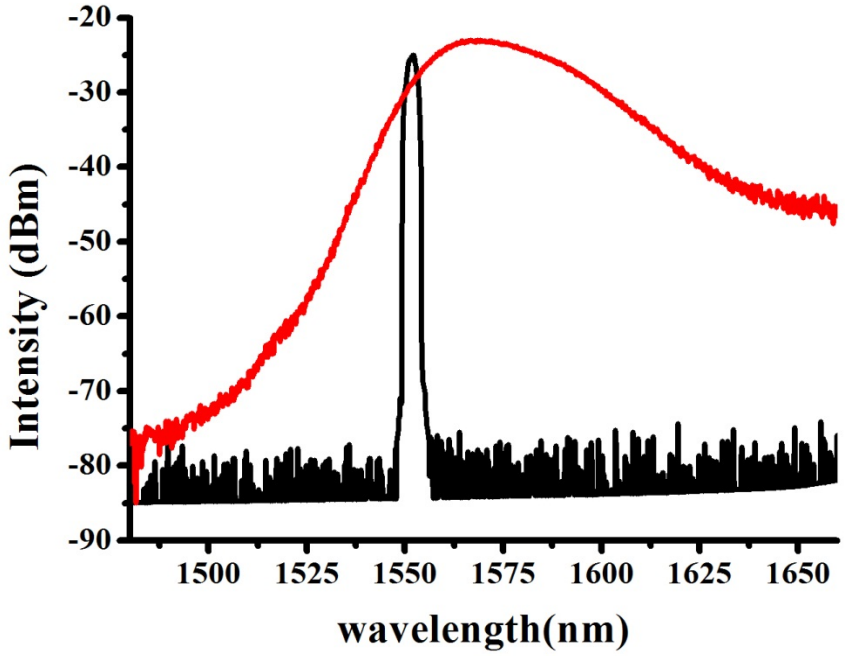

Fig. 3.30 Optical spectrum before (up) and after (down) filtering.

(left edge remain)

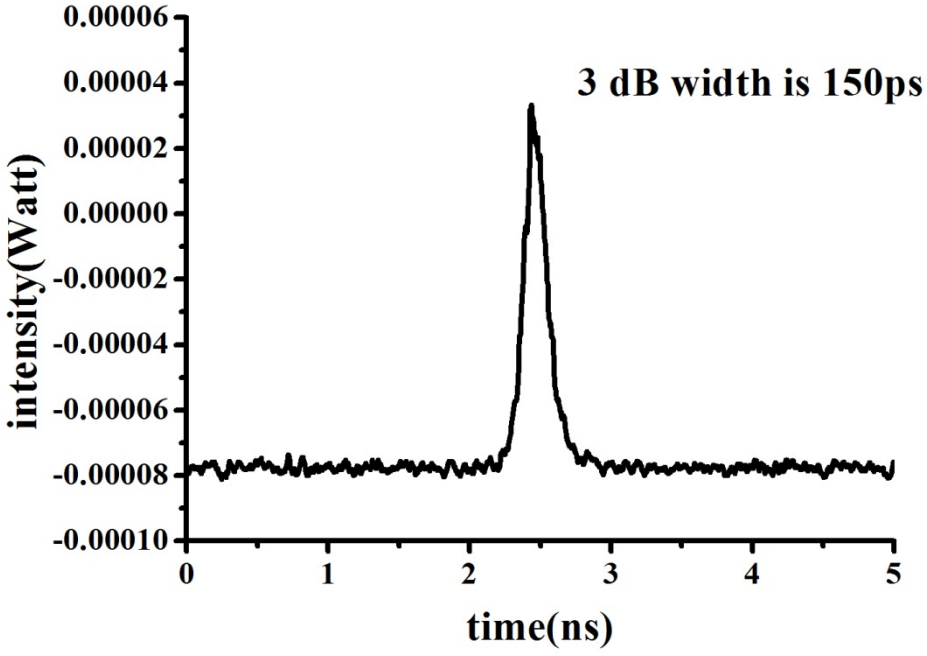

Fig. 3.31 Time trace of single pulse

(left edge remain)

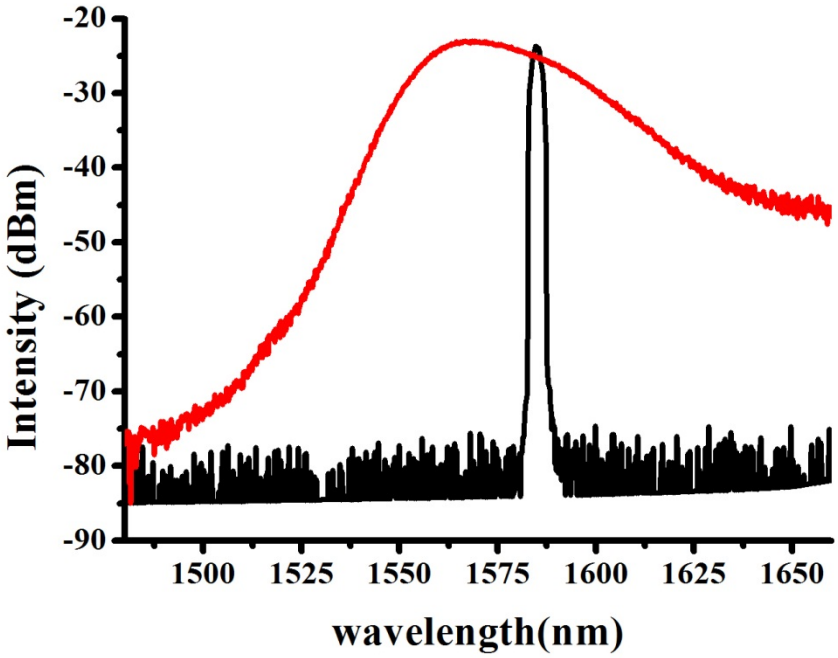

Fig. 3.32 Optical spectrum before (up) and after (down) filtering.

(right edge remain)

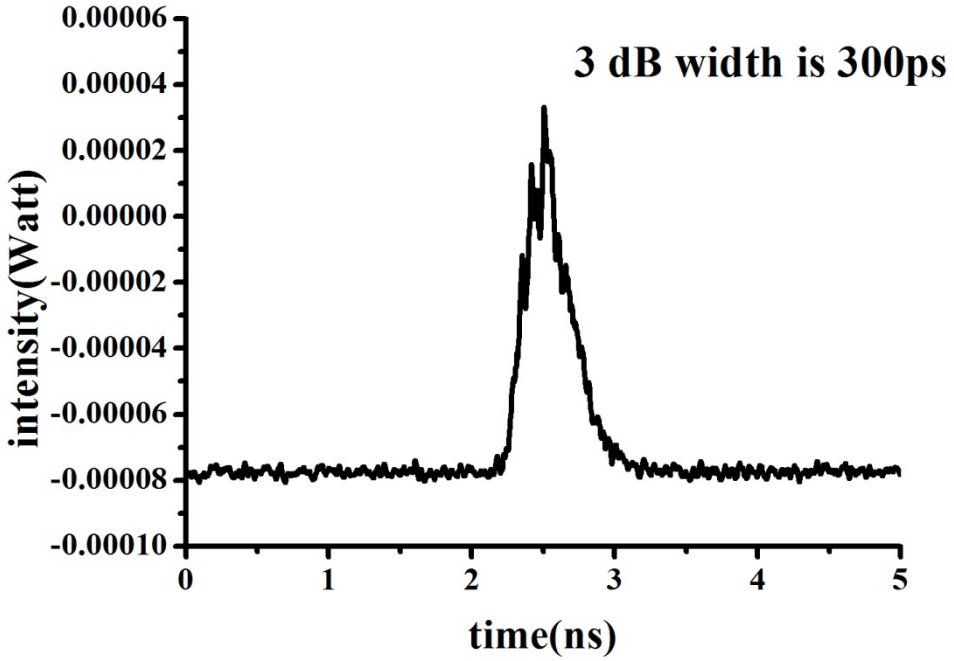

Fig. 3.33 Time trace of single pulse

(right edge remain)

After filtering, the measured pulse-width change apparently at different center wavelengths. It is due to the reason that the chirp coefficient of the pulse varies at different center wavelengths, and thus the pulse-width will change at different filtered center wavelengths [3.3]. Fig. 3.32 shows the filtered pulse-width versus different center wavelengths. The pulse-width increases almost linearly as we change the center wavelength from shorter to longer edges and the measured shortest pulse-width is about 150 ps.

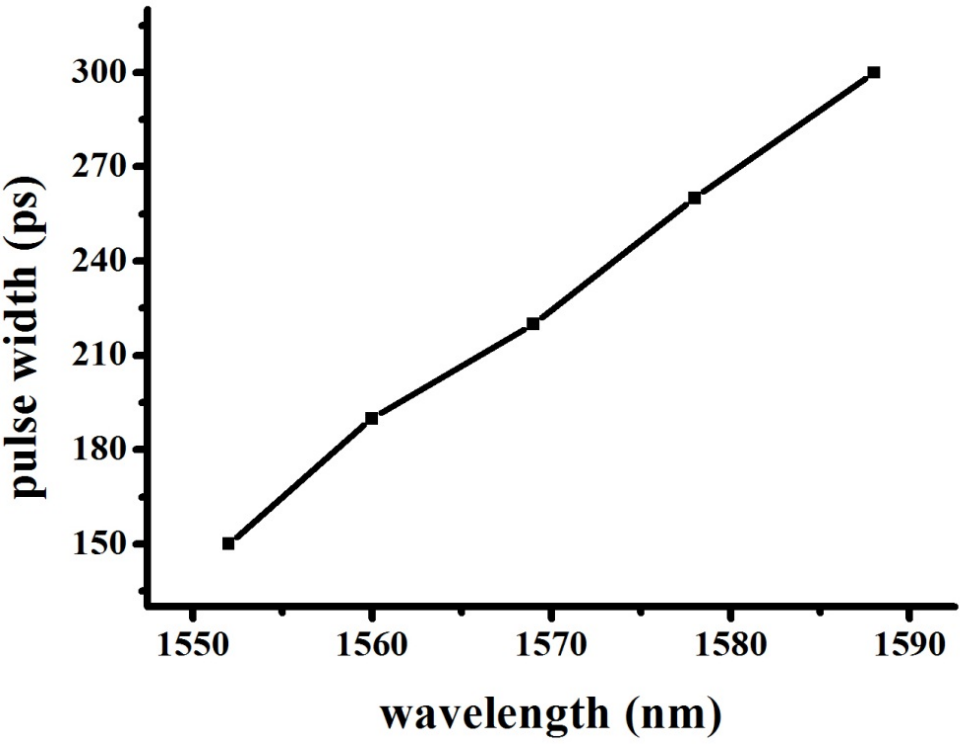

Fig. 3.34 Wavelength versus the pulse-width after filtering

Finally, through the filter-wavelength-dependent filtered pulse-width, the third order chirp parameter γ can be estimated. The resulting parameters are shown in Table 3.2

α	5.00458×10^{-27} (s^2)
δ	1.48699×10^{-23} (s^2)
γ	-7.52141×10^{-37} (s^3)

Table. 3.2 Estimated values of parameters

The characteristics of our laser outputs are now experimentally confirmed. In principle, we can use them to estimate the proper length of different characteristic fiber to further compress the output pulses.

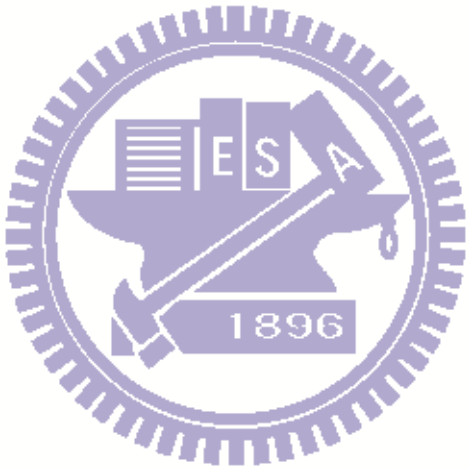

Reference

[3.1] A. Komarov, H. Leblond, and F. Sanchez, “Passive harmonic mode-locking in a fiber laser with nonlinear polarization rotation,” Opt. Communications 267, 162-169, 2006.

[3.2] L. E. Nelson, D. J. Jones, K. Tamura, H. A. Haus, and E. P. Ippen, “Ultrashort-pulse fiber ring lasers,” Appl. Phys. B, 65, 277–294, 1997.

[3.3] G. P. Agrawal, "Nonlinear Fiber Optics," fourth edition, Academic Press, San Diego, 2001.

Chapter 4

Conclusions

We have demonstrated a passive mode-locked all-fiber Er-doped fiber laser operated with large net round trip anomalous dispersion and large nonlinearity in a long fiber cavity. About 400 m single mode fibers have been added inside the laser cavity to generate stable wave-breaking-free pulses with 500 kHz repetition rate. At 561 mW pump power, the highest output power about 63 mW and highest pulse energy about 126 nJ have been experimtally demonstrated. Furthermore, a relatively broad and flat optical spectrum of 50 nm has been experimentally obtained with a 50/50 output coupler. This fiber laser configuration may be further applied to other applications that require a large pulse energy or peak power directly from the mode-locked fiber laser.

Nanosecond square profile pulses can also be generated in our laser system by proper adjustment of the PCs. At this state, the ML pulses can be maintained at relatively higher pump power without pulse breaking. It demonstrates that high energy pulses can not only generate in the net normal dispersion or all normal dispersion regions, but also in the large anomalous dispersion region. The pulse-width of square-shape pulses will become broadened as the pump power increases. It may be the reason for the observed pulse-breaking-free large pulse energy generation.

Finally, the characteristic parameters of the laser output pulses are experimentally estimated. It should help to design the external pulse compression setup for further reducing the pulse width. This will be one of our future research directions.